Physics Letters B 846 (2023) 137782

Contents lists available at ScienceDirect

Physics Letters B

journal homepage: www.elsevier.com/locate/physletb

Measurements of azimuthal anisotropies at forward and backward rapidity with muons in high-multiplicity p–Pb collisions at $\sqrt{s_{\rm NN}} = 8.16$ TeV

ALICE Collaboration *

ARTICLE INFO

Article history:
Received 26 October 2022
Received in revised form 30 January 2023
Accepted 15 February 2023
Available online 15 September 2023
Editor: M. Doser

Dataset link: https://www.hepdata.net/record/ins2165935

ABSTRACT

The study of the azimuthal anisotropy of inclusive muons produced in p–Pb collisions at $\sqrt{s_{\rm NN}} = 8.16$ TeV, using the ALICE detector at the LHC is reported. The measurement of the second-order Fourier coefficient of the particle azimuthal distribution, v_2, is performed as a function of transverse momentum $p_{\rm T}$ in the 0–20% high-multiplicity interval at both forward ($2.03 < y_{\rm CMS} < 3.53$) and backward ($-4.46 < y_{\rm CMS} < -2.96$) rapidities over a wide $p_{\rm T}$ range, $0.5 < p_{\rm T} < 10$ GeV/c, in which a dominant contribution of muons from heavy-flavour hadron decays is expected at $p_{\rm T} > 2$ GeV/c. The v_2 coefficient of inclusive muons is extracted using two different techniques, namely two-particle cumulants, used for the first time for heavy-flavour measurements, and forward–central two-particle correlations. Both techniques give compatible results. A positive v_2 is measured at both forward and backward rapidities with a significance larger than 4.7σ and 7.6σ, respectively, in the interval $2 < p_{\rm T} < 6$ GeV/c. Comparisons with previous measurements in p–Pb collisions at $\sqrt{s_{\rm NN}} = 5.02$ TeV, and with AMPT and CGC-based theoretical calculations are discussed. The findings impose new constraints on the theoretical interpretations of the origin of the collective behaviour in small collision systems.

1. Introduction

The study of high-energy heavy-ion collisions aims at investigating the properties of a state of strongly-interacting matter characterised by high energy density and temperature, called the quark–gluon plasma (QGP) [1,2]. One of the key observables to address the transport properties of the QGP is the azimuthal anisotropy of produced particles [3]. In non-central collisions, the initial spatial anisotropy of the overlap region is converted into an anisotropy in momentum space via multiple interactions. The magnitude of the azimuthal anisotropies is usually quantified via a Fourier decomposition of the particle azimuthal distribution given by

$$\frac{{\rm d}^2N}{{\rm d}p_{\rm T}{\rm d}\varphi} = \frac{1}{2\pi}\frac{{\rm d}N}{{\rm d}p_{\rm T}}\left(1 + 2\sum_{n=1}^{\infty} v_n(p_{\rm T})\cos[n(\varphi - \Psi_n)]\right), \quad (1)$$

where φ and $p_{\rm T}$ are the particle azimuthal angle and transverse momentum, respectively. The Fourier coefficients v_n characterise the anisotropy of produced particles [4] and Ψ_n is the azimuthal angle of the symmetry plane for the $n^{\rm th}$ harmonic. The largest contribution to the asymmetry of non-central collisions is provided by the second Fourier coefficient v_2 referred to as elliptic flow, and is expressed as $v_2 = \langle\cos[2(\varphi - \Psi_2)]\rangle$ [3,4], where the brackets denote the average over all particles and all selected events.

Due to their large masses, heavy quarks (charm and beauty) are mostly produced via hard partonic scattering processes in the very early stage of the collisions before the formation of the QGP, and therefore they probe the properties and dynamics of the QGP through its full evolution [5]. During their propagation through the medium, they lose energy via elastic and inelastic processes. Heavy-flavour hadrons and their decay products are thus sensitive probes of the QGP medium. The open heavy-flavour v_2 coefficient is expected to provide information on the collective expansion of the medium and thermalisation of heavy quarks at low $p_{\rm T}$ [3,6], and is sensitive to the path-length dependence of the in-medium energy loss at high $p_{\rm T}$ [7,8]. These contributions are predicted to give positive v_2 values. Moreover, the elliptic flow is also expected to be sensitive to the hadronisation processes at low and intermediate $p_{\rm T}$ [9,10]. Extensive measurements of the elliptic flow of heavy flavours have been carried out in Pb–Pb collisions at a centre-of-mass energy $\sqrt{s_{\rm NN}} = 2.76$ and 5.02 TeV at the LHC, and in Au–Au collisions at $\sqrt{s_{\rm NN}} = 200$ GeV at the RHIC [11] where

* *E-mail address:* alice-publications@cern.ch.

https://doi.org/10.1016/j.physletb.2023.137782

a positive elliptic flow coefficient was observed, see Refs. [12–24] for results on open heavy flavours. The nuclear modification factor R_{AA}, defined as the ratio of the particle yields in nucleus–nucleus (AA) collisions at the same centre-of-mass energy to that in binary-scaled pp collisions, is also an important observable to quantify in-medium effects. In addition to the non-zero v_2 coefficient, the R_{AA} measurements in heavy-ion collisions at LHC energies show a strong suppression of the open heavy-flavour yields at intermediate and high p_T [12,17,22,25–37]. These results reflect significant energy losses of heavy quarks due to strong interactions with the medium constituents.

The study of small collision systems such as p–Pb collisions at the LHC was initially proposed to address cold nuclear matter (CNM) effects relevant for the interpretation of the measurements in heavy-ion collisions, such as the nuclear modification of the parton distribution functions [38], k_T broadening [39], and energy loss in cold nuclear matter [40]. Surprisingly, long-range structures in two-particle correlations ("ridges") associated with a positive v_2 were first observed for light-flavour hadrons in high-multiplicity p–Pb collisions at $\sqrt{s_{NN}} = 5.02$ TeV in the midrapidity region by the ALICE, ATLAS, and CMS collaborations [41–46] and at forward rapidity by the LHCb collaboration [47], using the two-particle azimuthal correlation method. In the heavy-flavour sector, the ALICE and CMS collaborations revealed also hints of collectivity with the measurement of a positive v_2 of inclusive muons [48], inclusive and prompt J/ψ [49,50], prompt and non-prompt D mesons [51–54], and electrons from heavy-flavour hadron decays [55], using two-particle correlations. A positive v_2 of muons from heavy-flavour hadron decays was measured by ATLAS in high-multiplicity pp collisions at $\sqrt{s_{NN}}$ = 13 TeV [56] as well. Long-range correlations were also observed at lower beam energies, in d–Au [57–59] and ^{3}He–Au collisions [60], by the PHENIX and STAR collaborations at RHIC. Finally, the PHENIX collaboration studied the pseudorapidity (η) dependence of the charged-particle v_2 at high multiplicity in various asymmetric collision systems [61] as well. The v_2 signal was found to increase from the smallest to the largest system, and was also more pronounced in the backward rapidity region ($-3 < \eta < -1$) than at forward rapidity ($1 < \eta < 3$). Several strategies were developed to subtract the correlations not related to collectivity but rather due to jet correlations and resonance decays, referred to as nonflow effects. These nonflow contributions were usually suppressed by requiring a pseudorapidity separation between particles forming the pair and by subtracting correlations measured in low-multiplicity collisions [42,62]. Later on, a standard template fit procedure [63] was implemented to isolate the long-range correlations, which was further corrected to consider the multiplicity dependence of the Fourier coefficients v_n [64]. It was also observed that multi-particle cumulants [45,65–70] strongly suppress nonflow correlations.

On the other hand, the simultaneous observation of a positive v_2 and particle yields compatible with those in binary-scaled pp collisions, i.e. a nuclear modification factor $R_{pPb} \sim 1$, for high-p_T charged particles measured in high-multiplicity p–Pb collisions at $\sqrt{s_{NN}} = 5.02$ TeV, is also puzzling [63,71,72]. As reported in Ref. [63], a jet quenching calculation with two different initial geometries [73] slightly underestimates the measured v_2 and fails in describing the R_{pPb} data which are in favour of no significant energy loss effects. Several other possible scenarios (see a review in Ref. [74]) relying either on final-state effects involving a hydrodynamic evolution of the produced particles [75–77] or initial-state effects such as gluon saturation in the framework of the colour glass condensate (CGC) [74,78,79], are investigated. Colour-charge exchanges in the final state [78] or the anisotropic escape of partons from the surface of the interaction region [80] might also contribute to the flow-like effects evidenced in small collision systems. A MultiPhase Transport (AMPT) model [81–83] addresses non-equilibrium dynamics and provides a microscopic evolution of parton interactions, hence including also the parton escape mechanism. The latter scenario is further investigated using the string-melting version of the AMPT model [83], employed here for the comparison with the data (see Section 4). In this version, the initial strings are converted into partons and the interactions are described via a parton cascade model [84]. The partons are then combined into hadrons via a spatial quark coalescence model and the rescatterings between hadrons are described by a relativistic transport (ART) model [85].

In order to shed more light on the origin of the azimuthal anisotropies in small systems, this letter presents new results concerning the v_2 coefficient of inclusive muons in high-multiplicity p–Pb collisions at $\sqrt{s_{NN}} = 8.16$ TeV with the ALICE detector at the LHC. These measurements are performed at forward ($2.03 < y_{CMS} < 3.53$) and backward ($-4.46 < y_{CMS} < -2.96$) rapidities and cover the transverse momentum interval $0.5 < p_T < 10$ GeV/c. They are obtained in a significantly extended p_T range dominated by decays of heavy-flavour hadrons at $p_T > 2$ GeV/c. The total uncertainties are reduced by a factor up to about 2.1 and 1.3 at forward and backward rapidities, respectively, compared to the previous ALICE muon results in p–Pb collisions at $\sqrt{s_{NN}} = 5.02$ TeV in the interval $0.5 < p_T < 4$ GeV/c [48]. Various analysis methods which exhibit different sensitivity to nonflow effects, are implemented to measure the p_T-differential v_2 of inclusive muons. The two-particle correlation method and the two-particle cumulants with generic framework [86], the latter applied for the first time for heavy-flavour v_2 measurements with ALICE, are used. In order to reduce nonflow contributions, a novel procedure based on the subtraction of correlations measured in low-multiplicity events is developed.

The letter is organised as follows. Section 2 presents the ALICE apparatus with an emphasis on the detectors used in the analysis and the data taking conditions. Section 3 contains a description of the flow methods and a presentation of the analysis details. Section 4 presents the results, namely the p_T-differential muon v_2 at forward and backward rapidities, measured using several multiplicity estimators with the two-particle correlation and two-particle cumulant methods. Comparisons with published measurements performed at $\sqrt{s_{NN}} = 5.02$ TeV in various kinematic regions are reported. Detailed comparisons with model calculations based on the colour glass condensate and AMPT predictions are also discussed. A summary and concluding remarks are given in Section 5.

2. Experimental apparatus and data samples

A detailed description of the ALICE apparatus and its performance can be found in Refs. [87,88]. The main subdetectors used in the analysis are presented in the following. The analysis uses muons reconstructed in the muon spectrometer which covers the pseudorapidity interval $-4.0 < \eta < -2.5$. The muon spectrometer consists of a 10 nuclear interaction length (λ_I) absorber in front of five tracking stations, each composed of two planes of cathode pad chambers, with the central one inside a dipole magnet of 3 Tm integrated field. The tracking system is completed with two trigger stations, each equipped with two planes of resistive plate chambers, behind a 1.2 m thick iron wall (7.2 λ_I). The latter stops secondary hadrons escaping from the front absorber as well as low momentum muons from light-hadron decays. A conical absorber protects the muon spectrometer throughout its full length against secondary particles produced by the interaction with the beam pipe of primary particles at large η. Among the central barrel detectors, the two innermost layers of the Inner Tracking System composing the Silicon Pixel Detector (SPD) cover the pseudorapidity intervals $|\eta| < 2$ and $|\eta| < 1.4$. The SPD is employed for the determination of the position of the primary interaction ver-

tex. The SPD tracklets, track segments joining hits in the two SPD layers, are also used in the flow analysis, either as associated particles in the two-particle correlation method or to determine the reference flow with two-particle cumulants (Section 3). The V0 detector composed of two scintillator arrays, covers the pseudorapidity intervals $2.8 < \eta < 5.1$ (V0A) and $-3.7 < \eta < -1.7$ (V0C). It provides the minimum bias (MB) trigger defined by the coincidence of signals in the two sets of scintillators. The V0 is also used for the luminosity determination, and an independent measurement is obtained with the two T0 arrays of Cherenkov detectors located in the regions $4.6 < \eta < 4.9$ and $-3.3 < \eta < -3.0$. The two sets of Zero Degree Calorimeters (ZDC), each including a neutron calorimeter (ZN) and a proton calorimeter (ZP), are located on both sides of the interaction point at $z = \pm 112.5$ m, along the beam line. The timing information delivered by the V0 and ZDC is exploited offline to reject the beam-induced background. These two detectors are also used to estimate the event activity.

The results reported in this letter are obtained with the data samples recorded by ALICE during the 2016 p–Pb run at $\sqrt{s_{\rm NN}} = 8.16$ TeV, with two different beam configurations obtained by reversing the rotation direction of the proton and lead beams. Due to the asymmetry of the beam energy per nucleon, the nucleon-nucleon centre of mass is shifted in rapidity with respect to the laboratory frame by $\Delta y = 0.465$ in the direction of the proton beam. Therefore, inclusive muons are measured in the forward rapidity interval $2.03 < y_{\rm CMS} < 3.53$ with the proton beam travelling in the direction of the muon spectrometer (p-going direction, p–Pb configuration) and in the backward rapidity interval $-4.46 < y_{\rm CMS} < -2.96$ (Pb-going direction, Pb–p configuration). The analysis is based on muon-triggered events, requiring the MB condition and at least a track registered in the muon trigger stations with a $p_{\rm T}$ above a programmable threshold value. Data were collected with two programmable $p_{\rm T}$ thresholds set to about 0.5 GeV/c and 4.2 GeV/c, referred to as MSL and MSH, respectively. These two thresholds are not sharp, and correspond to a ∼50% efficiency for muons [89]. Based on statistical considerations, the measurement of the v_2 of inclusive muons is performed by combining MSL- and MSH-triggered events which are used up to $p_{\rm T} = 2$ GeV/c and above this value, respectively. It has been checked that in the overlapping region, both samples give same inclusive muon v_2 results within uncertainties. After applying an event selection which uses the information of the V0 and SPD together with an algorithm to tag events with multiple vertices, the pile-up contribution is found negligible for the data samples considered in this analysis. Moreover, only events with a primary vertex along the beam axis $z_{\rm vtx}$ within ±7 cm are considered in order to reduce non-uniform acceptance effects. After the event selection, the integrated luminosity of the p–Pb and Pb–p data samples corresponds to about 0.22 (5.8) nb^{-1} and 0.22 (8.2) nb^{-1} for MSL-(MSH-)triggered events, respectively. The p–Pb and Pb–p data samples are further classified according to their activity using multiplicity-based estimators [90] such as the total charge deposited in the two V0 arrays (V0M), the number of clusters in the outer layer of the SPD (CL1), and the energy deposited by spectator neutrons in the ZN located in the direction of the Pb beam. The ZN estimator minimises biases on the binary scaling of hard processes [90]. The multiplicity classes are defined as percentile intervals of the p–Pb and Pb–p hadronic cross section. In this analysis, the 0–20% and 60–90% multiplicity classes are studied. The evolution of the charged-particle pseudorapidity density at midrapidity in different multiplicity classes and with several multiplicity estimators is reported in Ref. [91].

The same selection criteria as in previous analyses [92,93] are applied to the muon candidates. Tracks in the muon spectrometer are reconstructed within the pseudorapidity region $-4 < \eta < -2.5$ to reject tracks at the edge of the muon spectrometer acceptance. The track polar angle at the end of the front absorber $\theta_{\rm abs}$ has to satisfy the condition $170^\circ < \theta_{\rm abs} < 178^\circ$ in order to remove tracks crossing the high-density region of the absorber that undergo significant scattering. Tracks reconstructed in the muon tracking chambers are identified as muons by requiring their matching with corresponding track segments in the muon trigger chambers. Finally, a selection on the minimum distance of the track to the primary vertex in the transverse plane (DCA) weighted by its momentum (p) is applied to reject fake tracks and remaining beam-induced background tracks. The SPD tracklets are selected in the fiducial region $|\eta| < 1$. Moreover, a condition on the pseudorapidity dependence on the longitudinal position of the primary vertex $z_{\rm vtx}$ is applied for the removal of edge effects in the region where the SPD acceptance is small. As in previous publications [48,49], a condition on the difference between the azimuthal angles of clusters in the two SPD layers with respect to the primary vertex, $\Delta\varphi_{\rm SPD} < 5$ mrad, is applied in order to select in average reference tracks with larger $p_{\rm T}$, which exhibit a larger flow, and to reduce the contribution from fake and secondary tracklets.

3. Analysis methods and associated systematic uncertainties

3.1. Two-particle correlations

The method using two-particle correlations to extract the azimuthal anisotropy is extensively discussed in Refs. [41–45,47–49,55]. The two-particle correlation between pairs of trigger particles, inclusive muons at forward or backward rapidities, and associated particles, SPD tracklets at midrapidity, is measured as a function of their azimuthal angle difference ($\Delta\varphi$) and pseudorapidity difference ($\Delta\eta$). The correlation is expressed in terms of Y, the associated yield per trigger particle defined as

$$Y = \frac{1}{N_{\rm trig}} \frac{{\rm d}^2 N_{\rm assoc}}{{\rm d}\Delta\eta {\rm d}\Delta\varphi} = \frac{S(\Delta\eta, \Delta\varphi)}{B(\Delta\eta, \Delta\varphi)}, \quad (2)$$

where $N_{\rm trig}$ is the total number of trigger particles, i.e. the number of inclusive muons in a given multiplicity class, $z_{\rm vtx}$ interval, and $p_{\rm T}$ interval. The signal distribution $S(\Delta\eta, \Delta\varphi)$ given by $\frac{1}{N_{\rm trig}} \frac{{\rm d}^2 N_{\rm same}}{{\rm d}\Delta\eta {\rm d}\Delta\varphi}$, corresponds to the associated yield per trigger particle for particle pairs from the same event. The background distribution $B(\Delta\eta, \Delta\varphi) = \alpha \frac{{\rm d}^2 N_{\rm mix}}{{\rm d}\Delta\eta {\rm d}\Delta\varphi}$ is obtained by correlating trigger particles in an event with associated particles from other events in the same multiplicity class and $z_{\rm vtx}$ interval. The parameter α is introduced to normalise the background distribution to unity in the region of maximum pair acceptance. Both the signal and background distributions are determined considering the same multiplicity class and same $z_{\rm vtx}$ interval of 1 cm width. The final associated yield per trigger particle is obtained from an average over the $z_{\rm vtx}$ intervals weighted by $N_{\rm trig}$.

The distribution of the associated yield per trigger particle (Eq. (2)) measured in high-multiplicity collisions is usually composed of correlations arising from collective and nonflow effects, the latter consisting of near-side ($|\Delta\varphi| < \pi/2$) and away-side ($\pi/2 < \Delta\varphi < 3\pi/2$) jet structures. These nonflow effects can be reduced by subtracting the per-trigger yield distribution measured in low-multiplicity collisions [42]. A typical example of associated yield per trigger particle for muon–tracklet correlations as a function of $\Delta\eta$ and $\Delta\varphi$ after the subtraction of the per-trigger yield measured in low-multiplicity (60–90%) collisions [42], labelled as $Y_{\rm sub}$, is shown in Fig. 1 (top-left panel) for high-multiplicity (0–20%) p–Pb collisions at $\sqrt{s_{\rm NN}} = 8.16$ TeV. The selected $p_{\rm T}$ interval of trigger particles is $2 < p_{\rm T} < 2.5$ GeV/c. A double-ridge

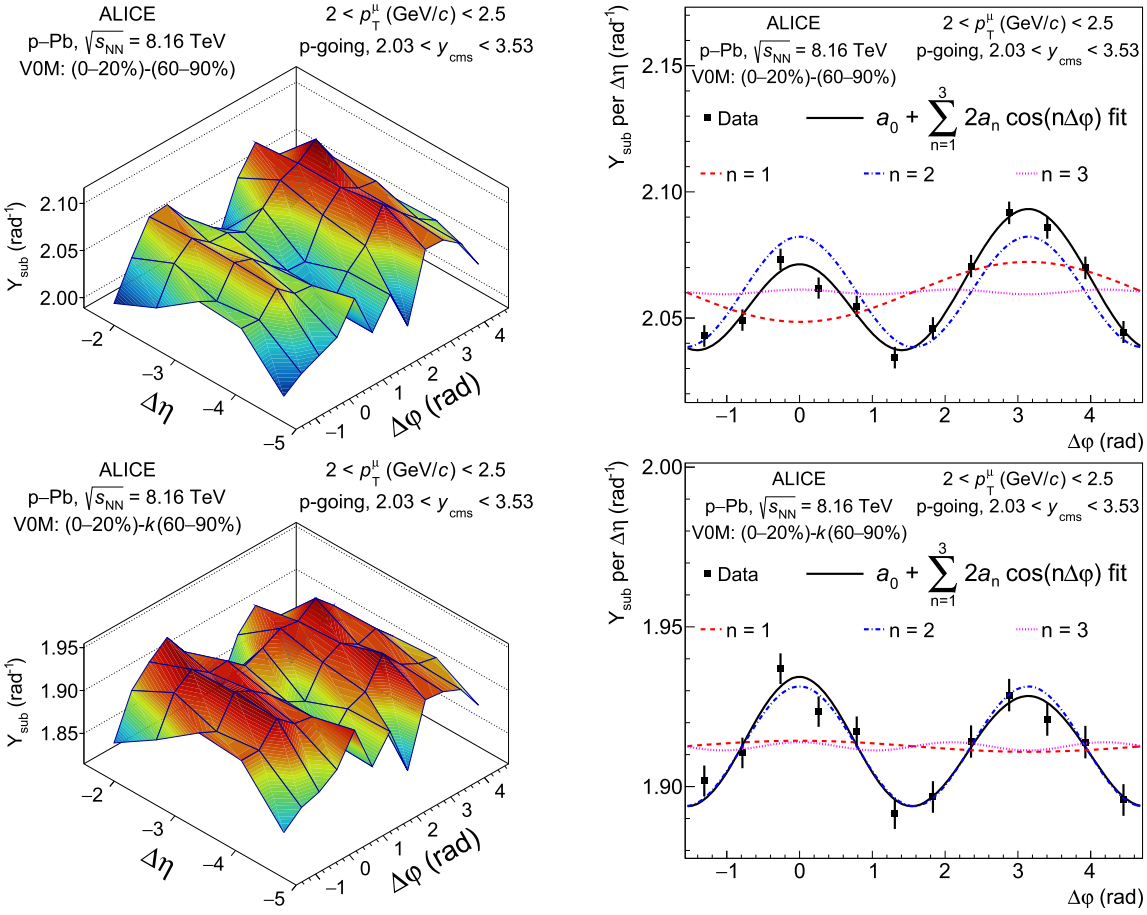

Fig. 1. Left: associated yield per trigger particle as a function of $\Delta\eta$ and $\Delta\varphi$ between inclusive muons with $2 < p_T < 2.5$ GeV/c and SPD tracklets, Y_{sub}, in high-multiplicity (0–20%) p–Pb collisions at $\sqrt{s_{NN}} = 8.16$ TeV after the subtraction of the unscaled (top) and scaled (bottom) muon–tracklet correlation in low-multiplicity (60–90%) events. Right: fit of the corresponding correlation distributions in $-5 < \Delta\eta < -1.5$ projected onto $\Delta\varphi$ with a Fourier decomposition, see Eq. (3). The three first harmonics are also presented.

structure is observed with a near-side ridge and a away-side ridge centred at $\Delta\varphi = 0$ and $\Delta\varphi = \pi$, respectively. This double-ridge structure indicates the presence of collective effects in p–Pb collisions. In order to quantify these remaining correlations, the resulting two-dimensional subtracted distribution in $-5 < \Delta\eta < -1.5$ is projected onto $\Delta\varphi$ and is further fitted with a Fourier series up to the third order

$$\frac{1}{N_{\text{trig}}}\frac{\mathrm{d}N_{\text{assoc}}}{\mathrm{d}\Delta\varphi} = a_0 + \sum_{n=1}^{3} 2a_n \cos(n\Delta\varphi), \tag{3}$$

where, as shown in Fig. 1 (top-right panel), an azimuthal anisotropy dominated by the second-order coefficient a_2 is observed.

After the subtraction of the muon–tracklet distribution measured in low-multiplicity collisions, the away-side jet yield in high-multiplicity collisions has strongly decreased. However, since the jet correlation is observed to be diminished in low-multiplicity collisions [94], a residual jet contamination in the subtracted distribution, in particular in the away side, is still present. The subtraction of this potential remaining jet component in the away side relies on the scaling of the low-multiplicity event class as described hereafter (see also Refs. [45,48,94]). The per-trigger associated yield in the low-multiplicity event class is first fitted with a Gaussian function centered at $\Delta\varphi = \pi$. The per-trigger yield in the high-multiplicity event class is further adjusted with Eq. (3) replacing the $\cos(\Delta\varphi)$ term by a Gaussian function whose width is fixed to the value obtained from the fit in low-multiplicity events. The per-trigger yield distribution in low-multiplicity events is scaled by a factor k defined as the ratio of the corresponding yields in the away side in high-multiplicity collisions to those in low-multiplicity collisions and the subtraction procedure is applied [48,49]. The k factors are larger in the p-going than in the Pb-going direction. They reach maximum values up to 1.43 (p-going) and 1.23 (Pb-going) with the V0M estimator. The values increase up to 1.74 (1.43) and 1.32 (1.0) in the p-going (Pb-going) direction, with the CL1 and ZN multiplicity estimators. Fig. 1 presents the resulting associated yield per trigger particle as a function of $\Delta\eta$ and $\Delta\varphi$ and the projected distribution onto $\Delta\varphi$ in bottom-left and bottom-right panels, respectively. One can notice that the amplitudes of the near-side and away-side ridges become comparable.

The subtraction of the scaled per-trigger yield in low-multiplicity collisions as well as the fit of the projected $\Delta\varphi$ distribution with Eq. (3) are repeated for each p_T trigger-particle interval. The values of the reduced χ^2 are all smaller than 1.5, confirming that the distributions are well described by this Fourier series. The $V_{n\Delta}^{\mu-\text{tracklet}}$ Fourier coefficients are further extracted from the fit parameters according to $V_{n\Delta}^{\mu-\text{tracklet}} = a_n/(a_0 + b)$, b corresponding to the baseline of the scaled 60–90% low-multiplicity class estimated from the integral in $\Delta\varphi$ of the correlation distribution around the minimum. By assuming that $V_{2\Delta}^{\mu-\text{tracklet}}$ can be factorised as the product of the anisotropies of single muons and SPD tracklets [62], the single muon second-order coefficient ($v_2^\mu\{2\text{PC}\}$) can be expressed as

$$v_2^{\mu}\{2\text{PC}\} = \frac{V_{2\Delta}^{\mu-\text{tracklet}}}{\sqrt{V_{2\Delta}^{\text{tracklet}-\text{tracklet}}}}. \quad (4)$$

In order to extract the $V_{2\Delta}^{\text{tracklet}-\text{tracklet}}$, the analysis is repeated by correlating only SPD tracklets, as also done in Refs. [42,44], and the region $|\Delta\eta| < 1.2$ is excluded to reduce a bias due to a possible remaining jet peak on the near side at ($\Delta\eta \sim 0$, $\Delta\varphi \sim 0$) after the subtraction of the correlation distribution in low-multiplicity collisions.

The systematic uncertainties affecting the $v_2^{\mu}\{2\text{PC}\}$ coefficient originate from the measurement of the muon–tracklet and tracklet–tracklet correlation distributions. They arise from the selection criteria of SPD tracklets, the procedure to remove the jet contamination in the near side and away side, the $v_2^{\mu}\{2\text{PC}\}$ calculation including the fit stability and baseline determination, and the effect of the muon-track resolution.

The effect of the SPD acceptance is investigated by varying the range of the position of the reconstructed vertex along the beam axis, which is decreased down to $|z_{\text{vtx}}| < 5$ cm.

The systematic effect related to the procedure implemented to subtract the jet contamination is investigated. A residual near-side jet peak in the tracklet–tracklet correlation is negligible since the $V_{2\Delta}^{\text{tracklet}-\text{tracklet}}$ coefficient remains unchanged when varying the $|\Delta\eta|$ gap in the range 0.8–1.2 units. The effect of a possible incomplete away-side jet subtraction is studied with the scaling procedure of the correlations in low-multiplicity collisions prior to its subtraction, as previously discussed. The influence of such an effect is also investigated fitting the subtracted correlation distributions, (0–20%) − (60–90%), with Eq. (3) replacing the first order term by a Gaussian function with the width fixed to the one extracted from the fit of correlations in low-multiplicity collisions in the away side. The differences between the two procedures give an estimation of the corresponding systematic uncertainty. A potential bias could result from long-range correlations remaining in the 60–90% low-multiplicity class, which may lead to an oversubtraction. Such effect is estimated by changing the multiplicity interval of the low-multiplicity event class from the nominal 60–90% to 70–90%.

The stability of the $v_2^{\mu}\{2\text{PC}\}$ results is also investigated by excluding the third-order coefficient in the fit of the muon–tracklet and track-tracklet correlations with Fourier series. The quality of the fits is getting worse, although no significant change in the extracted $v_2^{\mu}\{2\text{PC}\}$ values is seen. A systematic uncertainty also arises from the procedure employed for the $\Delta\varphi$ projection. The baseline is a parameter which could influence the fits and is estimated following the same strategy as in Ref. [48]. The latter is obtained by fitting the correlation distributions in low-multiplicity collisions using a Gaussian function in the away side and a constant for the baseline. Alternatively, the baseline can also be calculated in high-multiplicity collisions from the integral or from a second-order polynomial fit around the minimum at $\Delta\varphi \sim \pi/2$. Finally, the $\Delta\varphi$ projection is obtained from a constant fit instead of a first-order polynomial fit along $\Delta\eta$ for each $\Delta\varphi$ interval.

The systematic effect due to the angular and momentum resolution of reconstructed muon tracks is evaluated by means of a dedicated Monte Carlo simulation based on the DPMJET event generator [95], which uses the GEANT4 transport code [96,97] and the afterburner flow technique [98].

The various systematic uncertainties coming from each source are reported in Table 1 at forward (p-going) and backward (Pb-going) rapidities for the V0M multiplicity estimator. They are added in quadrature to obtain the overall systematic uncertainty on $v_2^{\mu}\{2\text{PC}\}$. Comparable uncertainty values are estimated in the 0–20% event class selected with CL1 and ZN multiplicity estimators.

Table 1
Summary of absolute systematic uncertainties affecting the $v_2^{\mu}\{2\text{PC}\}$ coefficients measured in high-multiplicity (0–20%) p–Pb collisions at $\sqrt{s_{\text{NN}}} = 8.16$ TeV in p-going and Pb-going directions. The values are reported for the event class selected with the V0M multiplicity estimator. The systematic uncertainties vary within the indicated intervals depending on the inclusive muon p_{T}.

Source	V0M	
	p-going ($\times 10^3$)	Pb-going ($\times 10^3$)
SPD acceptance	0.2–8.0	0.9–6.5
Residual jet	0.6–6.7	0.3–7.1
Remaining ridge in 60–90%	0.3–6.2	0.05–13.7
$v_2^{\mu}\{2\text{PC}\}$ calculation	0.2–1.7	0.4–3.4
Resolution effects	0.03–0.7	0.2–0.8
Total	1.5–10.7	1.4–17.1

3.2. Two-particle cumulants

Two-particle cumulants, which exhibit different sensitivities to nonflow compared to the two-particle correlation method, are also employed for the study of the second-order v_2 coefficient of inclusive muons [23]. For the first time in the heavy-flavour sector, the muon v_2 is measured with the two-particle cumulants using the framework presented in Ref. [86] where a method to correct for non-uniform acceptance and inefficiencies is provided. The SPD tracklets (reference particles, RP) are selected under the same selection criteria as with two-particle correlations. Apart from that, a more restrictive selection of the primary vertex position along the beam direction of $-5 < z_{\text{vtx}} < 3$ cm is considered to account for dead zones in the SPD detector in the plane $z_{\text{vtx}} - \varphi$, which cannot be corrected with particle weights. The standard selections discussed in Section 3.1 are applied to identify muon tracks, the so-called particles of interest (POI). The two-particle second-order reference and p_{T}-differential cumulants, $c_2\{2\}$ and $d_2^{\mu}\{2\}(p_{\text{T}})$, are based on the construction of weighted Q and p vectors[1] [86], defined on an event-by-event basis for a given multiplicity class and data sample (MSL- or MSH-triggered events) as

$$Q_{\text{n,l}} = \sum_{\text{k}=1}^{M} w_{\text{k}}^{\text{l}}(\eta, \varphi, z_{\text{vtx}}) e^{\text{i}(\text{n}\varphi_{\text{k}})} \text{ and}$$

$$p_{\text{n,l}} = \sum_{\text{k}=1}^{m_{\text{p}}} w_{\text{k}}^{\text{l}}(p_{\text{T}}, \eta, \varphi, z_{\text{vtx}}) e^{\text{i}(\text{n}\varphi_{\text{k}})}, \quad (5)$$

where n is the n^{th} harmonic number, l is an integer exponent of the k^{th}-particle (RP or POI) weight w_{k}^{l}, M is the multiplicity of the SPD tracklets, m_{p} is the muon multiplicity, and φ_{k} is the SPD tracklet (muon) azimuthal angle needed for the computation of $Q_{\text{n,l}}$ ($p_{\text{n,l}}$). After applying the weights for both SPD tracklets and inclusive muons, the non-uniformities in the azimuthal acceptance and inefficiencies are found negligible.

The calculation of the p_{T}-differential second-order coefficient of inclusive muons $v_2^{\mu}\{2\}$ in a given multiplicity interval is performed as

$$v_2^{\mu}\{2\}(p_{\text{T}}) = \frac{d_2^{\mu}\{2\}(p_{\text{T}})}{\sqrt{c_2\{2\}}}, \quad (6)$$

$c_2\{2\}$ being related to the reference second-order coefficient $V_2\{2\}$ as

$$V_2\{2\} = \sqrt{c_2\{2\}}. \quad (7)$$

[1] Since no autocorrelations between RP and POI are present, the $q_{\text{n,l}}$-vector constructed with only particles labeled both as RP and POI is not needed in the analysis.

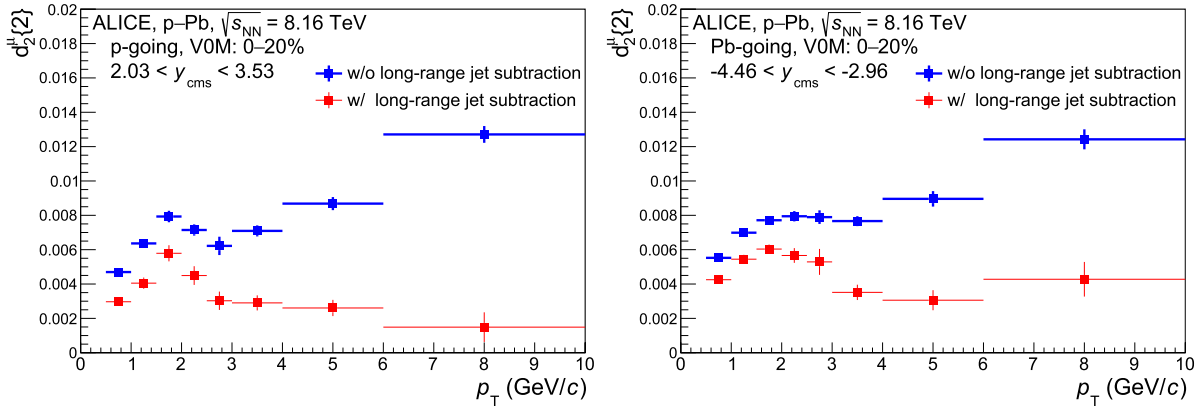

Fig. 2. Comparison of the two-particle second-order p_T-differential muon cumulant before and after the subtraction of the p_T-differential cumulant in low-multiplicity collisions and remaining long-range jet correlations at forward (left) and backward (right) rapidities in high-multiplicity p–Pb collisions at $\sqrt{s_{NN}} = 8.16$ TeV. The comparison is presented with the V0M estimator. Only statistical uncertainties are shown.

The measurement of the muon p_T-differential second-order coefficient with two-particle cumulants is influenced by nonflow effects which need to be isolated and subtracted. The $v_2^\mu\{2\}$ coefficient can be extracted from the equation

$$v_2^\mu\{2\}(p_T) = \frac{[d_2^\mu\{2\}(p_T)]_{(0-20\%)} - f \cdot g \cdot [d_2^\mu\{2\}(p_T)]_{(60-90\%)}}{f_{RP} \cdot \sqrt{[c_2\{2\}]_{(0-20\%)} - f \cdot [c_2\{2\}]_{(60-90\%)}}} \cdot f_{\Delta\eta}. \quad (8)$$

As done in the two-particle correlation method [48], the long-range jet correlations are estimated in the low-multiplicity event class 60–90%. Then, the two-particle second-order reference and differential cumulants in these low-multiplicity collisions are scaled by a factor f defined as the ratio of the mean SPD-tracklet multiplicity in low-multiplicity collisions to that in high-multiplicity collisions and subtracted as shown in Eq. (8). Short-range jet correlations are usually suppressed applying a pseudorapidity gap between the correlated particles, i.e. for both muons and SPD tracklets. As a pseudorapidity gap between muons and SPD tracklets is naturally present, the procedure cannot be applied straightforwardly for SPD tracklets due to the dead zones in the SPD acceptance. Therefore, these nonflow effects are suppressed via the scaling of the muon $v_2^\mu\{2\}$ by another factor, $f_{\Delta\eta}$, estimated by means of AMPT simulations [81,99] and defined as the ratio of $v_2^\mu\{2\}$ extracted with $|\Delta\eta| > 0.4$ to that obtained without applying a pseudorapidity gap. The optimised condition $|\Delta\eta| > 0.4$ results from a compromise between statistical considerations and suppression of nonflow effects. The value of this scaling factor is about 1.2 and is found to be independent of p_T and the multiplicity estimator.

As already discussed with the technique of two-particle correlations (see Section 3.1), remaining long-range jet correlations are not excluded even after the subtraction of correlations in low-multiplicity collisions. These remaining jet correlations can be suppressed by applying two additional correction factors. The factor g, applied to the p_T-differential cumulants measured in low-multiplicity collisions, is estimated from the muon–tracklet correlation distribution as discussed in Section 3.1. The factor f_{RP}, applied to $V_2\{2\}$, is calculated from the tracklet–tracklet correlation function. This is the ratio of $V_2\{2\}$ from tracklet–tracklet correlations extracted with the scaling of the remaining jet contribution to that obtained without any scaling procedure.

Fig. 2 presents the two-particle second-order p_T-differential muon cumulant in high-multiplicity (0–20%) collisions without and with the subtraction of the scaled p_T-differential muon cumulant in low-multiplicity collisions and remaining long-range jet correlations at forward (left) and backward (right) rapidities, using V0M for the multiplicity estimation. Large deviations appear at high p_T, indicating the importance to subtract long-range jet correlations at both forward and backward rapidities. These trends could result from the larger long-range jet contamination in the p-fragmentation region (forward rapidity, left panel) compared to the Pb-fragmentation region (backward rapidity, right panel) at high p_T, in particular. A similar behaviour is also seen with CL1 and ZN multiplicity estimators.

Several potential sources of systematic uncertainties affecting the measurement of the $v_2^\mu\{2\}$ coefficient are considered.

The non-uniform acceptance correction for SPD tracklets is expected to be independent of the analysed data sample. It is tested with the MB and muon-triggered samples. The difference of the results obtained with muon-triggered events with respect to the MB sample is taken as the corresponding systematic uncertainty.

The sensitivity of the results to the selection criteria of SPD tracklets is investigated by varying the η interval of SPD tracklets from $|\eta| < 1$ to $|\eta| < 1.2$.

The systematic uncertainty related to the procedure implemented for the subtraction of short-range jet correlations includes two components. A first contribution to the systematic uncertainty comes from the variation of the pseudorapidity gap up to $|\Delta\eta| > 0.8$. A second contribution is obtained conservatively from the comparison of the $v_2^\mu\{2\}$ computed with the scaling factor $f_{\Delta\eta}$ estimated from AMPT simulations and the measured one, using $|\Delta\eta| > 0$ ignoring that the effects due to non-uniformities in the azimuthal acceptance depend on z_{vtx}. In order to study the uncertainty from the away-side jet subtraction in the calculation of the p_T-differential cumulant, the subtracted p_T-differential cumulant, $[d_2^\mu\{2\}(p_T)]_{(0-20\%)} - f \cdot [d_2^\mu\{2\}(p_T)]_{(60-90\%)}$, i.e. the numerator of Eq. (8) with g set to unity, is scaled by a factor derived from the two-particle correlation method. This factor is estimated as the ratio of the $V_{2\Delta}^{\mu-\text{tracklet}}$ extracted fitting the subtracted correlation with Eq. (3) to that obtained replacing the first order term with the Gaussian function discussed in Section 3.1.

The systematic effect coming from the possible influence of long-range correlations in low-multiplicity events is assessed by changing the low-multiplicity interval from 60–90% to 70–90%.

Finally, the systematic uncertainty related to the angular and momentum resolution of the muon spectrometer is evaluated following the same strategy as with two-particle correlations (see Section 3.1).

The overall systematic uncertainty of $v_2^\mu\{2\}$ is evaluated summing in quadrature the various systematic uncertainties coming

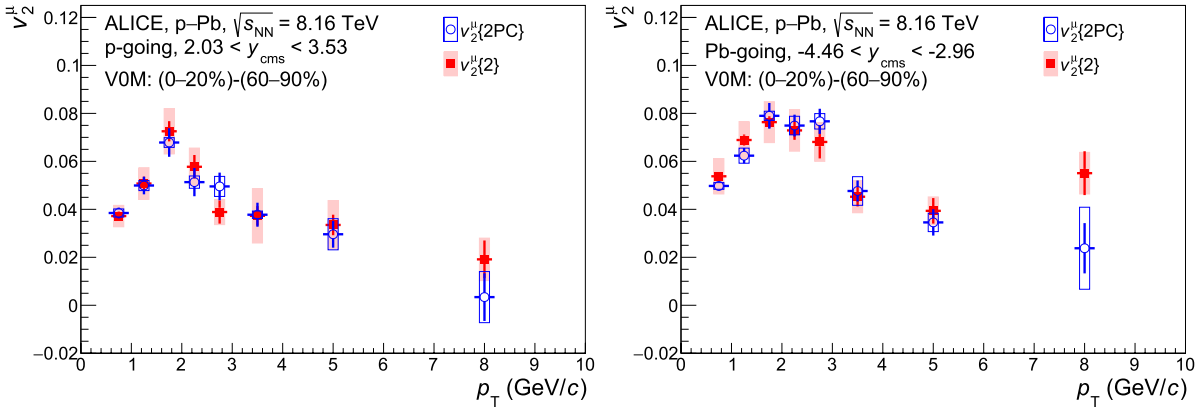

Fig. 3. Inclusive muon v_2^μ as a function of p_T at forward (left) and backward (right) rapidities in high-multiplicity p–Pb collisions at $\sqrt{s_{NN}} = 8.16$ TeV. The event activity is estimated with the V0M estimator. Open and full symbols refer to the measurements with two-particle correlations and two-particle cumulants, respectively.

Table 2
Summary of absolute systematic uncertainties affecting the $v_2^\mu\{2\}$ coefficients measured in high-multiplicity (0–20%) p–Pb collisions at $\sqrt{s_{NN}} = 8.16$ TeV in p-going and Pb-going directions. The values are reported for the event class selected with the V0M mutiplicity estimator. The systematic uncertainties vary within the indicated intervals depending on the inclusive muon p_T.

Source	V0M	
	p-going ($\times 10^3$)	Pb-going ($\times 10^3$)
Trigger bias	0.06–4.3	0.04–1.2
SPD acceptance	1.3–4.3	1.6–4.4
Short-range jet correlations: $\|\Delta\eta\|$ gap	0.9–3.6	1.3–2.5
Short-range jet correlations: $\|\Delta\eta\|$ data vs. AMPT	1.8–7.1	3.8–7.4
Residual jet	0.2–6.6	1.5–5.1
Remaining ridge in 60–90%	0.4–9.5	0.1–3.1
Resolution effects	0.2–0.7	0.4–0.8
Total	4.5–11.3	5.8–8.7

from each source. These uncertainties are summarised in Table 2 at both forward (p-going) and backward (Pb-going) rapidities for the V0M multiplicity estimator. The systematic uncertainties of $v_2^\mu\{2\}$ determined with CL1 or ZN mutiplicity estimators follow the same trends as a function of p_T and their values are compatible.

4. Results and model comparisons

Fig. 3 presents the p_T-differential second-order coefficient v_2^μ of inclusive muons after the subtraction of nonflow effects in the 0–20% high-multiplicity class for p–Pb collisions at $\sqrt{s_{NN}} = 8.16$ TeV. The results at forward and backward rapidities are depicted in the left and right panel, respectively. They are reported for the first time in a wide transverse momentum interval $0.5 < p_T < 10$ GeV/c. The event activity is determined with the V0M multiplicity estimator. Comparisons with the v_2^μ coefficient of inclusive muons measured in high-multiplicity events selected using CL1 and ZN multiplicity estimators will be discussed later. The measurements are carried out with two-particle correlations (open symbols) and two-particle cumulants (full symbols), which are denoted $v_2^\mu\{2PC\}$ and $v_2^\mu\{2\}$, respectively. The statistical uncertainties (vertical bars) with the two-particle cumulants are estimated according to the Jackknife method [100]. The latter is based on the resampling technique, where 6 out of 12 sub-samples are used to extract the RMS of the distribution for each p_T interval which is further divided by $\sqrt{2}$ in order to obtain the statistical uncertainty. In the two-particle correlation method, the statistical uncertainty is obtained from the Fourier fit procedure. The systematic uncertainties are the empty and filled boxes.

The two methods give compatible results within uncertainties at both forward and backward rapidities. One observes first an increase of the v_2^μ signal with increasing p_T where it reaches a maximum value of about 0.07 (0.08) at $p_T \sim 2$ GeV/c in the forward (backward) rapidity region, followed by a decrease as p_T increases. Although the p_T dependence is similar in the two rapidity regions, there is a hint for a higher elliptic flow signal at backward rapidity than at forward rapidity as observed in Ref. [48]. This is further investigated by the measurement of the p_T-differential ratio of the measured $v_2^\mu\{2PC\}$ at backward rapidity to that at forward rapidity. This ratio exhibits a uniform behaviour within uncertainties and can be fitted with a constant function (not shown here). It amounts to 1.28 ± 0.07, the uncertainty being from the fit. This asymmetry could be a consequence of decorrelation effects of the flow vectors in different rapidity regions [101–104].

In the p_T interval of interest, muons originate mainly from charged-pion and kaon decays at low p_T ($p_T < 2$ GeV/c), while muons from heavy-flavour hadron decays dominate over muons from light-hadron decays at higher p_T [48]. The contributions of these muon sources are estimated by means of simulations using the DMPJET event generator [95] and the GEANT4 transport package [96]. The relative contribution of muons from primary charged-pion and kaon decays amounts to about 67% (68%) at $0.5 < p_T < 1$ GeV/c, and it decreases with increasing p_T down to about 7.5% (14.5%) at $6 < p_T < 10$ GeV/c in the p-going (Pb-going) direction. The fraction of muons originating from charm and beauty decays represents about 60% (58%) of the total muon yield at $p_T = 2$ GeV/c and it reaches about 87% (78%) in the p-going (Pb-going) direction at $6 < p_T < 10$ GeV/c. A similar fraction of muons from heavy-flavour hadron decays in $0.5 < p_T < 4$ GeV/c is

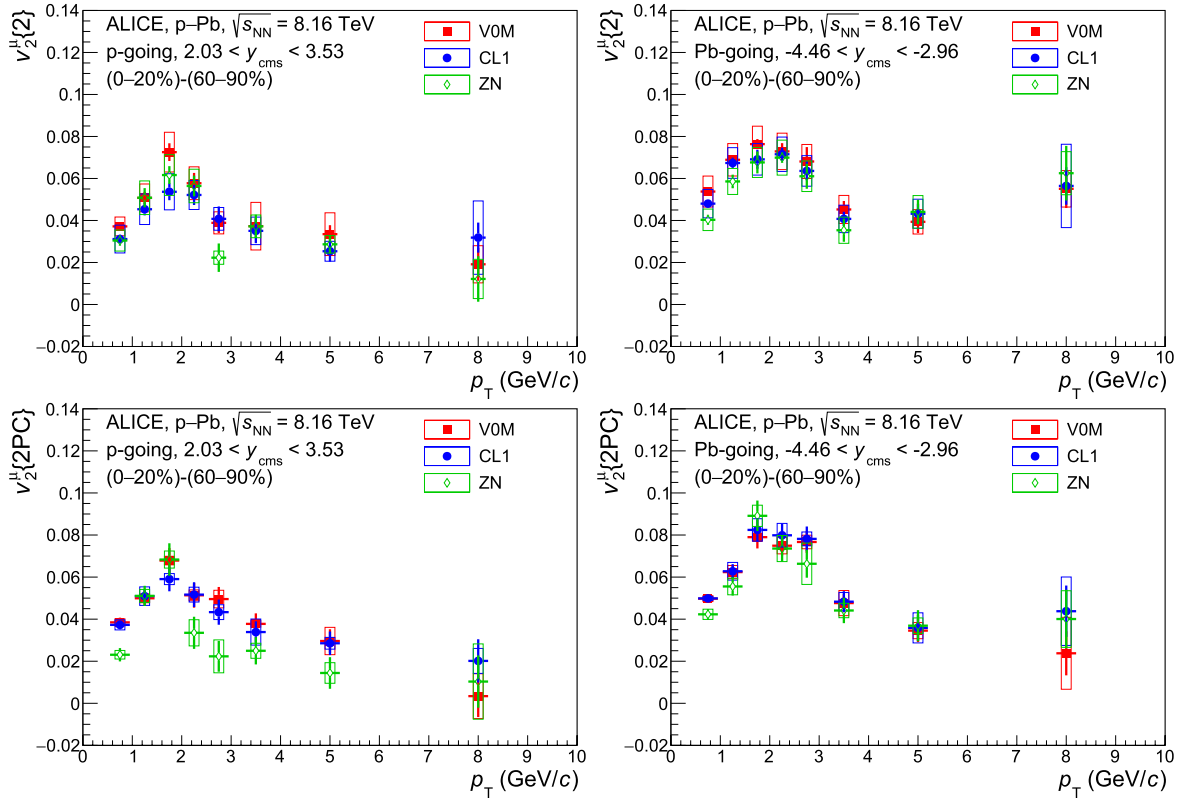

Fig. 4. Inclusive muon v_2^{μ} as a function of p_T at forward (left) and backward (right) rapidity in high-multiplicity p–Pb collisions at $\sqrt{s_{NN}} = 8.16$ TeV, extracted with two-particle cumulants (top) and two-particle correlations (bottom). The results are obtained with three different estimators of the event activity: V0M, CL1 and ZN.

reported for p–Pb collisions at $\sqrt{s_{NN}} = 5.02$ TeV [48]. Moreover, it is worth to mention that based on fixed-order plus next-to-leading logarithms (FONLL) calculations [105,106] more than 60% of muons from heavy-hadron decays originate from beauty quarks in the highest p_T interval ($6 < p_T < 10$ GeV/c). The measured v_2^{μ} coefficient is positive with a significance which reaches values of 4.7σ–12σ (7.6σ–11.9σ) at intermediate p_T ($2 < p_T < 6$ GeV/c) in the forward (backward) rapidity region, depending on the analysis technique. These results might suggest the existence of a collective behaviour of heavy quarks in high-multiplicity (0–20%) p–Pb collisions at $\sqrt{s_{NN}} = 8.16$ TeV at forward and backward rapidities. In the highest p_T interval accessible in this analysis ($6 < p_T <$ 10 GeV/c), where muons from beauty-hadron decays take over charm as the dominant muon component, there is a hint for a positive v_2^{μ} although not significant within uncertainties (significance of 0.2σ (1.2σ) at forward (backward) rapidity with two-particle correlations).

The analysis is repeated using the number of clusters in the outer layer of the SPD (CL1) and the energy deposited in the neutron ZDC (ZN) for the event activity selection. Fig. 4 displays the measurements obtained with two-particle cumulants (top panels) and two-particle correlations (bottom panels) at forward (left panels) and backward (right panels) rapidities. It has been demonstrated that these multiplicity estimators select different event classes associated with different mean charged-particle multiplicity [71]. The ZN is expected to be the least-biased estimator (see Section 2 and Ref. [90]) but the correlation between the energy measured with the ZDC and the charged-particle multiplicity at midrapidity is known to be weak [71]. On the other hand, autocorrelation effects are present when using CL1 for the event class selection (Section 2) since the reference flow is also calculated with the SPD tracklets. Even in this context, the computed v_2^{μ} values are compatible within uncertainties, although there is a hint for smaller v_2^{μ} values with the ZN multiplicity estimator than with V0M and CL1 multiplicity estimators. The ZN estimator selects on the average smaller charged-particle multiplicity density in the high-multiplicity class than V0M and CL1 estimators, while the opposite trend is observed for the low-multiplicity class [90,107]. Consequently, a smaller v_2^{μ} signal is expected after the subtraction of correlations from low-multiplicity events with the ZN estimator.

The present results are compared in Fig. 5 with previously published results of inclusive muons obtained by the ALICE collaboration in p–Pb collisions at $\sqrt{s_{NN}} = 5.02$ TeV with two-particle correlations [48]. The larger data sample collected at $\sqrt{s_{NN}} = 8.16$ TeV allows us to perform the measurements in a wider p_T interval, the p_T reach being extended from $p_T = 4$ GeV/c to $p_T = 10$ GeV/c. No significant $\sqrt{s_{NN}}$ dependence is seen on the extracted v_2 values at $\sqrt{s_{NN}} = 5.02$ TeV and 8.16 TeV in the interval $0.5 < p_T < 4$ GeV/c which contains a significant fraction of muons from light-hadron decays for $p_T < 2$ GeV/c. The results are also in good agreement within uncertainties with those obtained by ALICE for electrons from heavy-flavour hadrons measured in p–Pb collisions at $\sqrt{s_{NN}} = 5.02$ TeV at midrapidity ($-0.8 < \eta < 0.8$) and for $1.5 < p_T < 6$ GeV/c [55]. It is interesting to point out that the magnitude of the v_2 of inclusive muons is comparable within uncertainties to the one of inclusive muons obtained at forward rapidity by ALICE in semicentral Pb–Pb collisions at $\sqrt{s_{NN}} = 2.76$ TeV for $2 < p_T < 10$ GeV/c [23]. A positive v_2 also was reported by ALICE for J/ψ measured in $3 < p_T^{J/\psi} < 6$ GeV/c and same rapidity intervals in p–Pb collisions at $\sqrt{s_{NN}} = 8.16$ TeV, where the contribution from recombination of thermalised charm quarks in the medium is expected to be negligible and path-length dependent effects are smaller with respect to Pb–Pb collisions [49]. The present inclusive muon v_2 results also complement those obtained

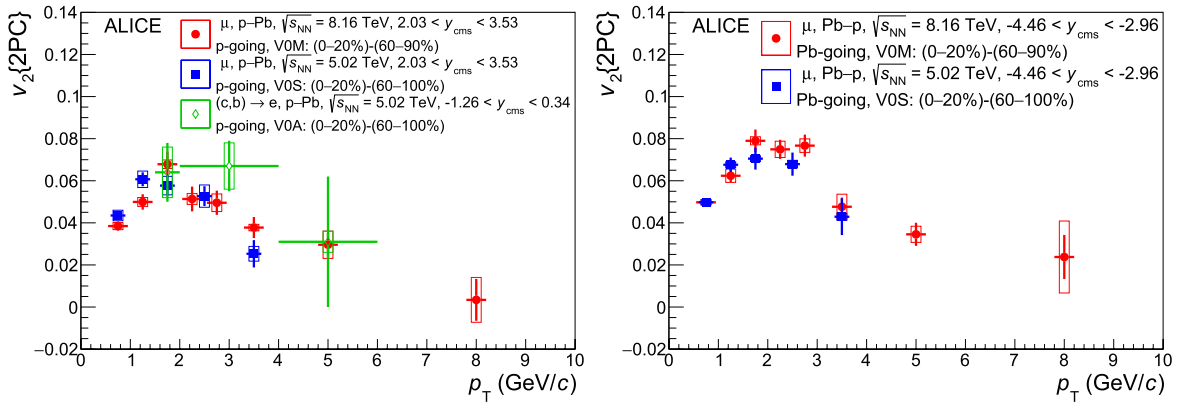

Fig. 5. Comparison of the p_T-differential v_2{2PC} of inclusive muons at forward (left) and backward (right) rapidity in high-multiplicity p–Pb collisions at $\sqrt{s_{NN}} = 8.16$ TeV, extracted with the two-particle correlation method with previous measurements performed in p–Pb collisions at $\sqrt{s_{NN}} = 5.02$ TeV for inclusive muons [48] and electrons from heavy-flavour hadron decays [55].

in high-multiplicity p–Pb collisions at $\sqrt{s_{NN}} = 5.02$ TeV for unidentified particles as well as pions, kaons and protons, although in a different kinematic region (different p_T and y intervals) [108,109].

Further insights in the understanding of the observed azimuthal anisotropies in small collision systems can be gained by comparing the measurements with model predictions such as the AMPT and colour glass condensate (CGC) calculations. The v2-26t7b string-melting version of the AMPT model [81,82] which includes the improvements discussed in Ref. [83] is employed to compute the v_2 of heavy-flavour hadrons (D^0 and B mesons) and primary charged pions and kaons by means of the forward–central two-particle corrections (Section 3.1). The event selection is performed by counting the charged particles in the acceptance of the V0 detector. The v_2 coefficient is then computed separately for muons from charm hadrons, beauty hadrons, charged pions and charged kaons by means of fast simulations which use the input p_T and v_2 distributions of D^0 and B mesons, and primary charged pions and kaons, as well as PYTHIA 6.4 [110] for the decay kinematics. The D-meson species are assumed to have the same v_2 coefficient as D^0 mesons.[II] The p_T-differential inclusive muon v_2^{μ} is obtained from a weighted sum of the v_2 coefficient of muons from heavy-flavour hadron decays, $v_2^{\mu\leftarrow b,c}$, and the v_2 of muons from charged pion and kaon decays, $v_2^{\mu\leftarrow\pi,K}$, as $v_2^{\mu} = (1-f)\cdot v_2^{\mu\leftarrow b,c} + f\cdot v_2^{\mu\leftarrow\pi,K}$, f being the relative abundance of muons from the decay of charged pions and kaons estimated from Monte Carlo simulations with the DPMJET event generator [95]. Similarly, the $v_2^{\mu\leftarrow b,c}$ coefficient is computed as a weighted sum of the v_2 coefficient of muons of charm-hadron and beauty-hadron decays, $v_2^{\mu\leftarrow c}$ and $v_2^{\mu\leftarrow b}$, as $f^c\cdot v_2^{\mu\leftarrow c} + f^b\cdot v_2^{\mu\leftarrow b}$. The corresponding fractions of muons from charm-hadron and beauty-hadron decays with respect to the total yield of muons from heavy-flavour hadron decays, f^c and f^b, are obtained by means of the fixed-order plus next-to-leading logarithms (FONLL) approach [105,106].

Fig. 6 presents a comparison of the p_T-differential inclusive muon v_2^{μ}{2PC} with AMPT calculations, together with the different contributions of muons from charm- and beauty-hadron decays, separately, and muons from charged pion and kaon decays in the p-going (left) and Pb-going (right) direction. The AMPT model generates a positive v_2 for all particle species. Its magnitude increases significantly in the low-p_T region up to about 2–3.5 GeV/c depending on the decay particle. At higher p_T, the v_2 signal decreases smoothly with increasing p_T or saturates, except in the Pb-going direction where a slightly increase with p_T is seen for muons from beauty-hadron decays. In line with hydrodynamic calculations [112], the AMPT model predicts a larger v_2 for muons from charged-pion and kaon decays than for muons from heavy-flavour hadron decays at low p_T in high-multiplicity p–Pb collisions. As observed with the data, the calculated v_2^{μ} values with the AMPT model are larger in the backward rapidity region compared to the forward rapidity region, which may be a consequence of rapidity-dependent flow-vector fluctuations [101–104]. The AMPT predictions are in fair agreement with the measured inclusive muon v_2^{μ}, although the model tends to slightly overestimate the data in the backward rapidity region. It is important to note that finite $v_2^{\mu\leftarrow b,c}$ values are indeed needed to reach such agreement. These AMPT comparisons suggest that the azimuthal anisotropies are mainly driven by the anisotropic parton escape mechanism where partons have a higher probability to escape along the shorter axis of the interaction zone, as discussed in Ref. [80].

Fig. 7 (left) shows a comparison of the measured p_T-differential muon v_2^{μ}{2PC} coefficient at forward rapidity with calculations based on the colour glass condensate (CGC) framework. The latter uses the dilute-dense formalism [113,114] where interactions between partons from the proton projectile and dense gluons inside the target Pb nucleus at the early stage of the collision generate azimuthal anisotropies. The comparison is performed only for the p-going direction where the dilute-dense formalism is valid [115]. The predictions of the v_2 coefficient have been provided separately for D^0 and B mesons from two-particle correlations. The v_2 coefficient of muons from heavy-flavour hadron decays is further obtained implementing the same strategy as with the AMPT predictions. One observes that in these CGC-based calculations, the correlations in the initial state generate a significant v_2 signal for muons from charm-hadron decays. Its magnitude increases significantly up to $p_T = 2$ GeV/c where it reaches a maximum value of about 0.09, and it decreases smoothly with increasing p_T. The predicted v_2 signal of muons from beauty-hadron decays is less pronounced, the maximum being of about 0.03 at $p_T = 3$ GeV/c. In the highest p_T region, the v_2 coefficient of muons from charm-hadron decays is similar to that of muons from beauty-hadron decays. The CGC-based calculations for muons from both charm- and beauty-hadron decays reproduce qualitatively the measured v_2^{μ} coefficient of inclusive muons for $p_T > 2$ GeV/c. It is worth pointing out that the contribution of muons from pion and kaon decays which contributes significantly to the measured inclusive muon yield at low p_T ($p_T < 2$ GeV/c) is not considered in the model predictions, preventing to draw any conclusion about the

[II] The elliptic flow of prompt D^0, D^+, D^{*+}, and D_s^+ measured by ALICE in Pb–Pb collisions at $\sqrt{s_{NN}} = 5.02$ TeV is found to be compatible within uncertainties [111].

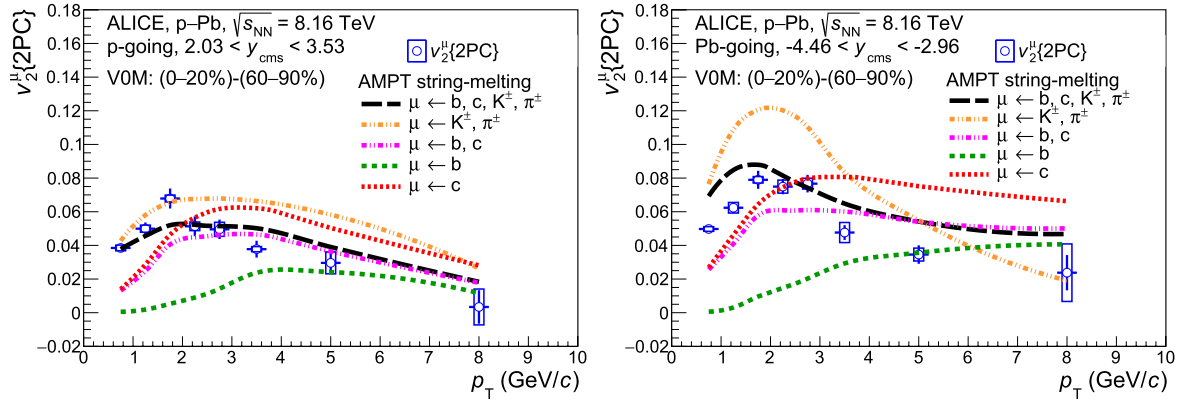

Fig. 6. Comparison of the p_T-differential v_2^μ{2PC} of inclusive muons at forward (left) and backward (right) rapidities in high-multiplicity p–Pb collisions at $\sqrt{s_{NN}} = 8.16$ TeV with AMPT calculations [81–83]. The predictions are shown for muons from charm-hadron decays and beauty-hadron decays, separately, muons from charged-pion and kaon decays, and for muons from the combination of the various sources. The contribution of muons from both charm- and beauty-hadron decays is also displayed.

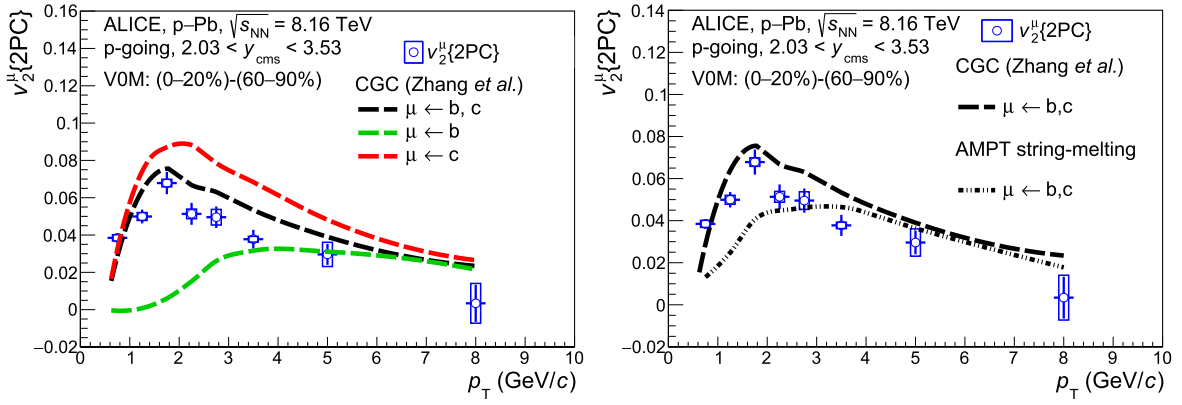

Fig. 7. Left: comparison of the p_T-differential v_2^μ{2PC} of inclusive muons at forward rapidity in high-multiplicity p–Pb collisions at $\sqrt{s_{NN}} = 8.16$ TeV with CGC-based calculations [113,114]. The predictions are shown for muons from charm-hadron decays and beauty-hadron decays, separately, and for muons from the combination of the two sources. Right: comparison of the p_T-differential v_2 of muons from heavy-flavour hadron decays as obtained with CGC and AMPT calculations with the measured inclusive muon v_2.

model comparisons in that kinematic region [48]. A similar agreement with these CGC calculations is found for prompt D^0, prompt J/ψ, and D^0 from beauty-hadron decays measured at midrapidity in p–Pb collisions at $\sqrt{s_{NN}} = 8.16$ TeV with the CMS detector [54]. The qualitative agreement between data and model calculations may suggest possible contributions from initial-state effects to the measured positive v_2 in high-multiplicity p–Pb collisions. However, it should be mentioned that the measured inclusive muon v_2^μ is obtained using charged particles for the calculation of the reference v_2 coefficient, which is in general interpreted as a final-state effect [103].

The CGC and AMPT predictions for muons from charm- and beauty-hadron decays are displayed together in the right panel of Fig. 7 for the p-going direction, and compared to the measured inclusive muon v_2^μ. The CGC-based calculations provide a larger v_2 signal for muons originating from heavy-flavour hadron decays at low p_T, up to about $p_T = 3$ GeV/c, compared to the AMPT calculations. Such behaviour indicates that the CGC calculations which do not incorporate muons from light-flavour hadron decays would have overestimated the data in this kinematic region. The two models provide compatible results and describe the data at high p_T, where the muons from charged-pion and kaon decays do not affect the v_2^μ significantly.

5. Conclusion

The second-order coefficient v_2^μ of inclusive muons in high-multiplicity p–Pb collisions at $\sqrt{s_{NN}} = 8.16$ TeV is measured with the ALICE detector at the LHC at forward ($2.03 < y_{CMS} < 3.53$) and backward ($-4.46 < y_{CMS} < -2.96$) rapidities. These new measurements extend previous inclusive muon ALICE results in p–Pb collisions at $\sqrt{s_{NN}} = 5.02$ TeV to a significantly broader transverse momentum interval of $0.5 < p_T < 10$ GeV/c. The v_2^μ coefficient is extracted using several event activity estimators with the well-known technique of two-particle correlations and, for the first time for open heavy-flavoured particles, with two-particle cumulants within the generic framework. Nonflow effects which cannot be neglected in the analyses involving correlations between two particles are subtracted using novel techniques. A positive v_2^μ signal is observed at forward and backward rapidities, with a significance larger than 4.7σ and 7.6σ, respectively, in the region $2 < p_T < 6$ GeV/c where muons from heavy-flavour hadron decays constitute the main source of muons. The results indicate that heavy quarks reveal a collective-like behaviour in high-multiplicity p–Pb collisions. The AMPT calculations which complement hydrodynamic models and address non-equilibrium dynamics provide a reasonable agreement with the data at both forward and backward rapidities over the whole p_T interval. The measured v_2^μ coefficient at forward rapidity (p-going direction) for $p_T > 2$ GeV/c is in qual-

itative agreement with CGC calculations within the dilute-dense formalism. Possible contributions from initial-state effects are not fully excluded at high p_{T}. These comprehensive results on v_2^{μ} of inclusive muons spanning in a wide p_{T} range, provide significant new insights for the understanding of the origin of the possible collective behaviour of heavy quarks in small systems such as p–Pb collisions and can be used to constrain the various approaches for modelling the azimuthal anisotropies in small collision systems.

Declaration of competing interest

The authors declare that they have no known competing financial interests or personal relationships that could have appeared to influence the work reported in this paper.

Data availability

This manuscript has associated data in a HEPData repository at: https://www.hepdata.net/record/ins2165935.

Acknowledgements

The authors would like to extend special thanks to Shu-Yi Wei for providing the CGC calculations and fruitful discussions.

The ALICE Collaboration would like to thank all its engineers and technicians for their invaluable contributions to the construction of the experiment and the CERN accelerator teams for the outstanding performance of the LHC complex. The ALICE Collaboration gratefully acknowledges the resources and support provided by all Grid centres and the Worldwide LHC Computing Grid (WLCG) collaboration. The ALICE Collaboration acknowledges the following funding agencies for their support in building and running the ALICE detector: A. I. Alikhanyan National Science Laboratory (Yerevan Physics Institute) Foundation (ANSL), State Committee of Science and World Federation of Scientists (WFS), Armenia; Austrian Academy of Sciences, Austrian Science Fund (FWF): [M 2467-N36] and Österreichische Nationalstiftung für Forschung, Technologie und Entwicklung, Austria; Ministry of Communications and High Technologies, National Nuclear Research Center, Azerbaijan; Conselho Nacional de Desenvolvimento Científico e Tecnológico (CNPq), Financiadora de Estudos e Projetos (Finep), Fundação de Amparo à Pesquisa do Estado de São Paulo (FAPESP) and Universidade Federal do Rio Grande do Sul (UFRGS), Brazil; Bulgarian Ministry of Education and Science, within the National Roadmap for Research Infrastructures 2020–2027 (object CERN), Bulgaria; Ministry of Education of China (MOEC), Ministry of Science & Technology of China (MSTC) and National Natural Science Foundation of China (NSFC), China; Ministry of Science and Education and Croatian Science Foundation, Croatia; Centro de Aplicaciones Tecnológicas y Desarrollo Nuclear (CEADEN), Cubaenergía, Cuba; Ministry of Education, Youth and Sports of the Czech Republic, Czech Republic; The Danish Council for Independent Research | Natural Sciences, the Villum Fonden and Danish National Research Foundation (DNRF), Denmark; Helsinki Institute of Physics (HIP), Finland; Commissariat à l'Énergie Atomique (CEA) and Institut National de Physique Nucléaire et de Physique des Particules (IN2P3) and Centre National de la Recherche Scientifique (CNRS), France; Bundesministerium für Bildung und Forschung (BMBF) and GSI Helmholtzzentrum für Schwerionenforschung GmbH, Germany; General Secretariat for Research and Technology, Ministry of Education, Research and Religions, Greece; National Research, Development and Innovation Office, Hungary; Department of Atomic Energy, Government of India (DAE), Department of Science and Technology, Government of India (DST), University Grants Commission, Government of India (UGC) and Council of Scientific and Industrial Research (CSIR), India; National Research and Innovation Agency - BRIN, Indonesia; Istituto Nazionale di Fisica Nucleare (INFN), Italy; Japanese Ministry of Education, Culture, Sports, Science and Technology (MEXT) and Japan Society for the Promotion of Science (JSPS) KAKENHI, Japan; Consejo Nacional de Ciencia (CONACYT) y Tecnología, through Fondo de Cooperación Internacional en Ciencia y Tecnología (FONCICYT) and Dirección General de Asuntos del Personal Académico (DGAPA), Mexico; Nederlandse Organisatie voor Wetenschappelijk Onderzoek (NWO), Netherlands; The Research Council of Norway, Norway; Commission on Science and Technology for Sustainable Development in the South (COMSATS), Pakistan; Pontificia Universidad Católica del Perú, Peru; Ministry of Education and Science, National Science Centre and WUT ID-UB, Poland; Korea Institute of Science and Technology Information and National Research Foundation of Korea (NRF), Republic of Korea; Ministry of Education and Scientific Research, Institute of Atomic Physics, Ministry of Research and Innovation and Institute of Atomic Physics and University Politehnica of Bucharest, Romania; Ministry of Education, Science, Research and Sport of the Slovak Republic, Slovakia; National Research Foundation of South Africa, South Africa; Swedish Research Council (VR) and Knut & Alice Wallenberg Foundation (KAW), Sweden; European Organization for Nuclear Research, Switzerland; Suranaree University of Technology (SUT), National Science and Technology Development Agency (NSTDA), Thailand Science Research and Innovation (TSRI) and National Science, Research and Innovation Fund (NSRF), Thailand; Turkish Energy, Nuclear and Mineral Research Agency (TENMAK), Turkey; National Academy of Sciences of Ukraine, Ukraine; Science and Technology Facilities Council (STFC), United Kingdom; National Science Foundation of the United States of America (NSF) and United States Department of Energy, Office of Nuclear Physics (DOE NP), United States of America. In addition, individual groups or members have received support from: Marie Skłodowska Curie, European Research Council, Strong 2020 - Horizon 2020 (grant nos. 950692, 824093, 896850), European Union; Academy of Finland (Center of Excellence in Quark Matter) (grant nos. 346327, 346328), Finland; Programa de Apoyos para la Superación del Personal Académico, UNAM, Mexico.

References

[1] B. Muller, J.L. Nagle, Results from the relativistic heavy ion collider, Annu. Rev. Nucl. Part. Sci. 56 (2006) 93–135, arXiv:nucl-th/0602029.
[2] A. Bazavov, et al., The chiral and deconfinement aspects of the QCD transition, Phys. Rev. D 85 (2012) 054503, arXiv:1111.1710 [hep-lat].
[3] J.-Y. Ollitrault, Anisotropy as a signature of transverse collective flow, Phys. Rev. D 46 (1992) 229–245.
[4] S. Voloshin, Y. Zhang, Flow study in relativistic nuclear collisions by Fourier expansion of Azimuthal particle distributions, Z. Phys. C 70 (1996) 665–672, arXiv:hep-ph/9407282.
[5] R. Averbeck, Heavy-flavor production in heavy-ion collisions and implications for the properties of hot QCD matter, Prog. Part. Nucl. Phys. 70 (2013) 159–209, arXiv:1505.03828 [nucl-ex].
[6] P.F. Kolb, U.W. Heinz, Hydrodynamic description of ultrarelativistic heavy ion collisions, arXiv:nucl-th/0305084.
[7] M. Gyulassy, I. Vitev, X. Wang, High p_{T} azimuthal asymmetry in noncentral A+A at RHIC, Phys. Rev. Lett. 86 (2001) 2537–2540, arXiv:nucl-th/0012092.
[8] E. Shuryak, The Azimuthal asymmetry at large p_{T} seems to be too large for a 'jet quenching', Phys. Rev. C 66 (2002) 027902, arXiv:nucl-th/0112042.
[9] V. Greco, C.M. Ko, R. Rapp, Quark coalescence for charmed mesons in ultrarelativistic heavy ion collisions, Phys. Lett. B 595 (2004) 202–208, arXiv:nucl-th/0312100 [nucl-th].
[10] D. Molnar, Charm elliptic flow from quark coalescence dynamics, J. Phys. G 31 (2005) S421–S428, arXiv:nucl-th/0410041.
[11] STAR Collaboration, L. Adamczyk, et al., Measurement of D^0 Azimuthal anisotropy at midrapidity in Au+Au collisions at $\sqrt{s_{\mathrm{NN}}}$=200 GeV, Phys. Rev. Lett. 118 (2017) 212301, arXiv:1701.06060 [nucl-ex].
[12] ALICE Collaboration, S. Acharya, et al., Measurement of prompt D_s^+-meson production and azimuthal anisotropy in Pb–Pb collisions at $\sqrt{s_{\mathrm{NN}}} = 5.02$TeV, Phys. Lett. B 827 (2022) 136986, arXiv:2110.10006 [nucl-ex].

[13] CMS Collaboration, A.M. Sirunyan, et al., Measurement of prompt D^0 and $\overline{D}^0$ meson azimuthal anisotropy and search for strong electric fields in PbPb collisions at $\sqrt{s_{NN}} = 5.02$ TeV, Phys. Lett. B 816 (2021) 136253, arXiv:2009.12628 [hep-ex].

[14] ATLAS Collaboration, G. Aad, et al., Measurement of azimuthal anisotropy of muons from charm and bottom hadrons in Pb+Pb collisions at $\sqrt{s_{NN}} = 5.02$ TeV with the ATLAS detector, Phys. Lett. B 807 (2020) 135595, arXiv:2003.03565 [nucl-ex].

[15] ALICE Collaboration, S. Acharya, et al., Elliptic flow of electrons from beauty-hadron decays in Pb–Pb collisions at $\sqrt{s_{NN}} = 5.02$ TeV, Phys. Rev. Lett. 126 (2021) 162001, arXiv:2005.11130 [nucl-ex].

[16] ALICE Collaboration, S. Acharya, et al., Transverse-momentum and event-shape dependence of D-meson flow harmonics in Pb–Pb collisions at $\sqrt{s_{NN}}$ = 5.02 TeV, Phys. Lett. B 813 (2021) 136054, arXiv:2005.11131 [nucl-ex].

[17] ATLAS Collaboration, M. Aaboud, et al., Measurement of the suppression and azimuthal anisotropy of muons from heavy-flavor decays in Pb+Pb collisions at $\sqrt{s_{NN}} = 2.76$ TeV with the ATLAS detector, Phys. Rev. C 98 (2018) 044905, arXiv:1805.05220 [nucl-ex].

[18] ALICE Collaboration, S. Acharya, et al., Event-shape engineering for the D-meson elliptic flow in mid-central Pb–Pb collisions at $\sqrt{s_{NN}} = 5.02$ TeV, J. High Energy Phys. 02 (2019) 150, arXiv:1809.09371 [nucl-ex].

[19] CMS Collaboration, A.M. Sirunyan, et al., Measurement of prompt D^0 meson azimuthal anisotropy in PbPb collisions at $\sqrt{s_{NN}} = 5.02$ TeV, Phys. Rev. Lett. 120 (2018) 202301, arXiv:1708.03497 [nucl-ex].

[20] ALICE Collaboration, S. Acharya, et al., D-meson azimuthal anisotropy in mid-central Pb–Pb collisions at $\sqrt{s_{NN}} = 5.02$ TeV, Phys. Rev. Lett. 120 (2018) 102301, arXiv:1707.01005 [nucl-ex].

[21] ALICE Collaboration, J. Adam, et al., Elliptic flow of electrons from heavy-flavour hadron decays at mid-rapidity in Pb–Pb collisions at $\sqrt{s_{NN}} = 2.76$ TeV, J. High Energy Phys. 09 (2016) 028, arXiv:1606.00321 [nucl-ex].

[22] CMS Collaboration, V. Khachatryan, et al., Suppression and azimuthal anisotropy of prompt and nonprompt J/ψ production in PbPb collisions at $\sqrt{s_{NN}} = 2.76$ TeV, Eur. Phys. J. C 77 (2017) 252, arXiv:1610.00613 [nucl-ex].

[23] ALICE Collaboration, J. Adam, et al., Elliptic flow of muons from heavy-flavour hadron decays at forward rapidity in Pb–Pb collisions at $\sqrt{s_{NN}} = 2.76$ TeV, Phys. Lett. B 753 (2016) 41–56, arXiv:1507.03134 [nucl-ex].

[24] ALICE Collaboration, B.B. Abelev, et al., Azimuthal anisotropy of D meson production in Pb–Pb collisions at $\sqrt{s_{NN}} = 2.76$ TeV, Phys. Rev. C 90 (2014) 034904, arXiv:1405.2001 [nucl-ex].

[25] ALICE Collaboration, S. Acharya, et al., Prompt D^0, D^+, and D^{*+} production in Pb–Pb collisions at $\sqrt{s_{NN}}$ = 5.02 TeV, J. High Energy Phys. 01 (2022) 174, arXiv:2110.09420 [nucl-ex].

[26] ATLAS Collaboration, G. Aad, et al., Measurement of the nuclear modification factor for muons from charm and bottom hadrons in Pb+Pb collisions at 5.02 TeV with the ATLAS detector, Phys. Lett. B 829 (2022) 137077, arXiv:2109.00411 [nucl-ex].

[27] ALICE Collaboration, S. Acharya, et al., Production of muons from heavy-flavour hadron decays at high transverse momentum in Pb–Pb collisions at $\sqrt{s_{NN}} = 5.02$ and 2.76 TeV, Phys. Lett. B 820 (2021) 136558, arXiv:2011.05718 [nucl-ex].

[28] ALICE Collaboration, S. Acharya, et al., Measurement of electrons from semileptonic heavy-flavour hadron decays at midrapidity in pp and Pb-Pb collisions at $\sqrt{s_{NN}} = 5.02$ TeV, Phys. Lett. B 804 (2020) 135377, arXiv:1910.09110 [nucl-ex].

[29] ALICE Collaboration, S. Acharya, et al., Measurements of low-p_T electrons from semileptonic heavy-flavour hadron decays at mid-rapidity in pp and Pb–Pb collisions at $\sqrt{s_{NN}} = 2.76$ TeV, J. High Energy Phys. 10 (2018) 061, arXiv:1805.04379 [nucl-ex].

[30] ALICE Collaboration, S. Acharya, et al., Measurement of D^0, D^+, D^{*+} and D_s^+ production in Pb-Pb collisions at $\sqrt{s_{NN}} = 5.02$ TeV, J. High Energy Phys. 10 (2018) 174, arXiv:1804.09083 [nucl-ex].

[31] CMS Collaboration, A.M. Sirunyan, et al., Studies of beauty suppression via nonprompt D^0 mesons in PbPb collisions at $Q^2 = 4$ GeV^2, Phys. Rev. Lett. 123 (2019) 022001, arXiv:1810.11102 [hep-ex].

[32] CMS Collaboration, A.M. Sirunyan, et al., Measurement of B_s^0 meson production in pp and PbPb collisions at $\sqrt{s_{NN}} = 5.02$ TeV, Phys. Lett. B 796 (2019) 168–190, arXiv:1810.03022 [hep-ex].

[33] ATLAS Collaboration, M. Aaboud, et al., Prompt and non-prompt J/ψ and $\psi(2S)$ suppression at high transverse momentum in 5.02 TeV Pb+Pb collisions with the ATLAS experiment, Eur. Phys. J. C 78 (2018) 762, arXiv:1805.04077 [nucl-ex].

[34] CMS Collaboration, A.M. Sirunyan, et al., Nuclear modification factor of D^0 mesons in PbPb collisions at $\sqrt{s_{NN}} = 5.02$ TeV, Phys. Lett. B 782 (2018) 474–496, arXiv:1708.04962 [nucl-ex].

[35] CMS Collaboration, A.M. Sirunyan, et al., Measurement of the $B^{\pm}$ meson nuclear modification factor in PbPb collisions at $\sqrt{s_{NN}} = 5.02$ TeV, Phys. Rev. Lett. 119 (2017) 152301, arXiv:1705.04727 [hep-ex].

[36] CMS Collaboration, A.M. Sirunyan, et al., Measurement of prompt and non-prompt charmonium suppression in PbPb collisions at 5.02 TeV, Eur. Phys. J. C 78 (2018) 509, arXiv:1712.08959 [nucl-ex].

[37] ALICE Collaboration, J. Adam, et al., Measurement of the production of high-p_T electrons from heavy-flavour hadron decays in Pb–Pb collisions at $\sqrt{s_{NN}}$ = 2.76 TeV, Phys. Lett. B 771 (2017) 467–481, arXiv:1609.07104 [nucl-ex].

[38] K.J. Eskola, H. Paukkunen, C.A. Salgado, EPS09: a new generation of NLO and LO nuclear parton distribution functions, J. High Energy Phys. 04 (2009) 065, arXiv:0902.4154 [hep-ph].

[39] B.Z. Kopeliovich, J. Nemchik, A. Schafer, A.V. Tarasov, Cronin effect in hadron production off nuclei, Phys. Rev. Lett. 88 (2002) 232303, arXiv:hep-ph/0201010 [hep-ph].

[40] Z.-B. Kang, I. Vitev, E. Wang, H. Xing, C. Zhang, Multiple scattering effects on heavy meson production in p+A collisions at backward rapidity, Phys. Lett. B 740 (2015) 23–29, arXiv:1409.2494 [hep-ph].

[41] CMS Collaboration, S. Chatrchyan, et al., Observation of long-range near-side angular correlations in proton-lead collisions at the LHC, Phys. Lett. B 718 (2013) 795–814, arXiv:1210.5482 [nucl-ex].

[42] ALICE Collaboration, B. Abelev, et al., Long-range angular correlations on the near and away side in pPb collisions at $\sqrt{s_{NN}} = 5.02$ TeV, Phys. Lett. B 719 (2013) 29–41, arXiv:1212.2001 [nucl-ex].

[43] ATLAS Collaboration, G. Aad, et al., Observation of associated near-side and away-side long-range correlations in $\sqrt{s_{NN}}$ = 5.02 TeV proton-lead collisions with the ATLAS detector, Phys. Rev. Lett. 110 (2013) 182302, arXiv:1212.5198 [hep-ex].

[44] ALICE Collaboration, B.B. Abelev, et al., Long-range angular correlations of π, K and p in p–Pb collisions at $\sqrt{s_{NN}}$ = 5.02 TeV, Phys. Lett. B 726 (2013) 164–177, arXiv:1307.3237 [nucl-ex].

[45] ATLAS Collaboration, M. Aaboud, et al., Measurements of long-range azimuthal anisotropies and associated Fourier coefficients for pp collisions at $\sqrt{s} = 5.02$ and 13 TeV and p+Pb collisions at $\sqrt{s_{NN}} = 5.02$ TeV with the ATLAS detector, Phys. Rev. C 96 (2017) 024908, arXiv:1609.06213 [nucl-ex].

[46] ALICE Collaboration, J. Adam, et al., Transverse momentum dependence of D-meson production in Pb–Pb collisions at $\sqrt{s_{NN}} = 2.76$ TeV, J. High Energy Phys. 03 (2016) 081, arXiv:1509.06888 [nucl-ex].

[47] LHCb Collaboration, R. Aaij, et al., Measurements of long-range near-side angular correlations in $\sqrt{s_{NN}} = 5$ TeV proton-lead collisions in the forward region, Phys. Lett. B 762 (2016) 473–483, arXiv:1512.00439 [nucl-ex].

[48] ALICE Collaboration, J. Adam, et al., Forward-central two-particle correlations in p–Pb collisions at $\sqrt{s_{NN}}$ = 5.02 TeV, Phys. Lett. B 753 (2016) 126–139, arXiv:1506.08032 [nucl-ex].

[49] ALICE Collaboration, S. Acharya, et al., Search for collectivity with azimuthal J/ψ-hadron correlations in high multiplicity p–Pb collisions at $\sqrt{s_{NN}}$ = 5.02 and 8.16 TeV, Phys. Lett. B 780 (2018) 7–20, arXiv:1709.06807 [nucl-ex].

[50] CMS Collaboration, A.M. Sirunyan, et al., Observation of prompt J/ψ meson elliptic flow in high-multiplicity pPb collisions at $\sqrt{s_{NN}} = 8.16$ TeV, Phys. Lett. B 791 (2019) 172–194, arXiv:1810.01473 [hep-ex].

[51] ALICE Collaboration, J. Adam, et al., Measurement of azimuthal correlations of D mesons and charged particles in pp collisions at $\sqrt{s} = 7$ TeV and p–Pb collisions at $\sqrt{s_{NN}} = 5.02$ TeV, Eur. Phys. J. C 77 (2017) 245, arXiv:1605.06963 [nucl-ex].

[52] ALICE Collaboration, S. Acharya, et al., Azimuthal correlations of prompt D mesons with charged particles in pp and p–Pb collisions at $\sqrt{s_{NN}}$ = 5.02 TeV, Eur. Phys. J. C 80 (2020) 979, arXiv:1910.14403 [nucl-ex].

[53] CMS Collaboration, A.M. Sirunyan, et al., Elliptic flow of charm and strange hadrons in high-multiplicity pPb collisions at $\sqrt{s_{NN}} = 8.16$ TeV, Phys. Rev. Lett. 121 (2018) 082301, arXiv:1804.09767 [hep-ex].

[54] CMS Collaboration, A.M. Sirunyan, et al., Studies of charm and beauty hadron long-range correlations in pp and pPb collisions at LHC energies, Phys. Lett. B 813 (2021) 136036, arXiv:2009.07065 [hep-ex].

[55] ALICE Collaboration, S. Acharya, et al., Azimuthal anisotropy of heavy-flavor decay electrons in p-Pb collisions at $\sqrt{s_{NN}}$ = 5.02 TeV, Phys. Rev. Lett. 122 (2019) 072301, arXiv:1805.04367 [nucl-ex].

[56] ATLAS Collaboration, G. Aad, et al., Measurement of azimuthal anisotropy of muons from charm and bottom hadrons in pp collisions at $\sqrt{s} = 13$ TeV with the ATLAS detector, Phys. Rev. Lett. 124 (2020) 082301, arXiv:1909.01650 [nucl-ex].

[57] PHENIX Collaboration, A. Adare, et al., Quadrupole anisotropy in dihadron Azimuthal correlations in central d+Au collisions at $\sqrt{s_{NN}}$ = 200 GeV, Phys. Rev. Lett. 111 (2013) 212301, arXiv:1303.1794 [nucl-ex].

[58] PHENIX Collaboration, A. Adare, et al., Measurement of long-range angular correlation and quadrupole anisotropy of pions and (anti)protons in central d+Au collisions at $\sqrt{s_{NN}}$ = 200 GeV, Phys. Rev. Lett. 114 (2015) 192301, arXiv:1404.7461 [nucl-ex].

[59] STAR Collaboration, L. Adamczyk, et al., Long-range pseudorapidity dihadron correlations in d+Au collisions at $\sqrt{s_{NN}} = 200$ GeV, Phys. Lett. B 747 (2015) 265–271, arXiv:1502.07652 [nucl-ex].

[60] PHENIX Collaboration, A. Adare, et al., Measurements of elliptic and triangular flow in high-multiplicity ^{3}He+Au collisions at $\sqrt{s_{NN}} = 200$ GeV, Phys. Rev. Lett. 115 (2015) 142301, arXiv:1507.06273 [nucl-ex].

[61] PHENIX Collaboration, A. Adare, et al., Pseudorapidity dependence of particle production and elliptic flow in asymmetric nuclear collisions of p+Al, p+Au,

d+Au, and ^{3}He+Au at $\sqrt{s_{\rm NN}} = 200$ GeV, Phys. Rev. Lett. 121 (2018) 222301, arXiv:1807.11928 [nucl-ex].

[62] ATLAS Collaboration, G. Aad, et al., Measurement of long-range pseudorapidity correlations and azimuthal harmonics in $\sqrt{s_{\rm NN}} = 5.02$ TeV proton-lead collisions with the ATLAS detector, Phys. Rev. C 90 (2014) 044906, arXiv:1409.1792 [hep-ex].

[63] ATLAS Collaboration, G. Aad, et al., Transverse momentum and process dependent azimuthal anisotropies in $\sqrt{s_{\rm NN}} = 8.16$ TeV p+Pb collisions with the ATLAS detector, Eur. Phys. J. C 80 (2020) 73, arXiv:1910.13978 [nucl-ex].

[64] ATLAS Collaboration, M. Aaboud, et al., Correlated long-range mixed-harmonic fluctuations measured in pp, p+Pb and low-multiplicity Pb+Pb collisions with the ATLAS detector, Phys. Lett. B 789 (2019) 444–471, arXiv:1807.02012 [nucl-ex].

[65] CMS Collaboration, V. Khachatryan, et al., Evidence for collective multiparticle correlations in pPb collisions, Phys. Rev. Lett. 115 (2015) 012301, arXiv:1502.05382 [nucl-ex].

[66] ATLAS Collaboration, M. Aaboud, et al., Measurement of multi-particle azimuthal correlations in pp, p+Pb and low-multiplicity Pb+Pb collisions with the ATLAS detector, Eur. Phys. J. C 77 (2017) 428, arXiv:1705.04176 [hep-ex].

[67] ATLAS Collaboration, M. Aaboud, et al., Measurement of long-range multiparticle azimuthal correlations with the subevent cumulant method in pp and p + Pb collisions with the ATLAS detector at the CERN large hadron collider, Phys. Rev. C 97 (2018) 024904, arXiv:1708.03559 [hep-ex].

[68] CMS Collaboration, A.M. Sirunyan, et al., Multiparticle correlation studies in pPb collisions at $\sqrt{s_{\rm NN}} = 8.16$ TeV, Phys. Rev. C 101 (2020) 014912, arXiv:1904.11519 [hep-ex].

[69] ALICE Collaboration, S. Acharya, et al., Investigations of anisotropic flow using multiparticle azimuthal correlations in pp, p-Pb, Xe-Xe, and Pb-Pb collisions at the LHC, Phys. Rev. Lett. 123 (2019) 142301, arXiv:1903.01790 [nucl-ex].

[70] ALICE Collaboration, B.B. Abelev, et al., Multiparticle azimuthal correlations in p–Pb and Pb–Pb collisions at the CERN large hadron collider, Phys. Rev. C 90 (2014) 054901, arXiv:1406.2474 [nucl-ex].

[71] ALICE Collaboration, J. Adam, et al., Centrality dependence of particle production in p-Pb collisions at $\sqrt{s_{\rm NN}}$ = 5.02 TeV, Phys. Rev. C 91 (2015) 064905, arXiv:1412.6828 [nucl-ex].

[72] ATLAS Collaboration, G. Aad, et al., Transverse momentum, rapidity, and centrality dependence of inclusive charged-particle production in $\sqrt{s_{\rm NN}} = 5.02$ TeV p + Pb collisions measured by the ATLAS experiment, Phys. Lett. B 763 (2016) 313–336, arXiv:1605.06436 [hep-ex].

[73] X. Zhang, J. Liao, Jet quenching and its azimuthal anisotropy in AA and possibly high multiplicity pA and dA collisions, arXiv:1311.5463 [nucl-th].

[74] K. Dusling, W. Li, B. Schenke, Novel collective phenomena in high-energy proton–proton and proton–nucleus collisions, Int. J. Mod. Phys. E 25 (2016) 1630002, arXiv:1509.07939 [nucl-ex].

[75] P. Bozek, Collective flow in p-Pb and d-Pb collisions at TeV energies, Phys. Rev. C 85 (2012) 014911, arXiv:1112.0915 [hep-ph].

[76] P. Bozek, W. Broniowski, Correlations from hydrodynamic flow in p–Pb collisions, Phys. Lett. B 718 (2013) 1557–1561, arXiv:1211.0845 [nucl-th].

[77] J.L. Nagle, W.A. Zajc, Small system collectivity in relativistic hadronic and nuclear collisions, Annu. Rev. Nucl. Part. Sci. 68 (2018) 211–235, arXiv:1801.03477 [nucl-ex].

[78] K. Dusling, R. Venugopalan, Evidence for BFKL and saturation dynamics from dihadron spectra at the LHC, Phys. Rev. D 87 (2013) 051502, arXiv:1210.3890 [hep-ph].

[79] K. Dusling, R. Venugopalan, Comparison of the color glass condensate to dihadron correlations in proton-proton and proton-nucleus collisions, Phys. Rev. D 87 (2013) 094034, arXiv:1302.7018 [hep-ph].

[80] L. He, T. Edmonds, Z.-W. Lin, F. Liu, D. Molnar, F. Wang, Anisotropic parton escape is the dominant source of azimuthal anisotropy in transport models, Phys. Lett. B 753 (2016) 506–510, arXiv:1502.05572 [nucl-th].

[81] Z.-W. Lin, C.M. Ko, B.-A. Li, B. Zhang, S. Pal, A multi-phase transport model for relativistic heavy ion collisions, Phys. Rev. C 72 (2005) 064901, arXiv:nucl-th/0411110.

[82] H. Li, Z.-W. Lin, F. Wang, Charm quarks are more hydrodynamic than light quarks in final-state elliptic flow, Phys. Rev. C 99 (2019) 044911, arXiv:1804.02681 [hep-ph].

[83] Z.-W. Lin, L. Zheng, Further developments of a multi-phase transport model for relativistic nuclear collisions, Nucl. Sci. Tech. 32 (2021) 113, arXiv:2110.02989 [nucl-th].

[84] B. Zhang, ZPC 1.0.1: a parton cascade for ultrarelativistic heavy ion collisions, Comput. Phys. Commun. 109 (1998) 193–206, arXiv:nucl-th/9709009.

[85] B.-A. Li, C.M. Ko, Formation of superdense hadronic matter in high-energy heavy ion collisions, Phys. Rev. C 52 (1995) 2037–2063, arXiv:nucl-th/9505016.

[86] A. Bilandzic, C.H. Christensen, K. Gulbrandsen, A. Hansen, Y. Zhou, Generic framework for anisotropic flow analyses with multiparticle azimuthal correlations, Phys. Rev. C 89 (2014) 064904, arXiv:1312.3572 [nucl-ex].

[87] ALICE Collaboration, K. Aamodt, et al., The ALICE experiment at the CERN LHC, J. Instrum. 3 (2008) S08002.

[88] ALICE Collaboration, B.B. Abelev, et al., Performance of the ALICE Experiment at the CERN LHC, Int. J. Mod. Phys. A 29 (2014) 1430044, arXiv:1402.4476 [nucl-ex].

[89] ALICE Collaboration, F. Bossu, M. Gagliardi, M. Marchisone, Performance of the RPC-based ALICE muon trigger system at the LHC, J. Instrum. 7 (2012) T12002, arXiv:1211.1948 [physics.ins-det].

[90] ALICE Collaboration, S. Acharya, et al., Charged-particle pseudorapidity density at mid-rapidity in p–Pb collisions at $\sqrt{s_{\rm NN}}$ = 8.16 TeV, Eur. Phys. J. C 79 (2019) 307, arXiv:1812.01312 [nucl-ex].

[91] ALICE Collaboration, S. Acharya, et al., Charged-particle pseudorapidity density at mid-rapidity in p-Pb collisions at $\sqrt{s_{\rm NN}}$ = 8.16 TeV, Eur. Phys. J. C 79 (2019) 307, arXiv:1812.01312 [nucl-ex].

[92] ALICE Collaboration, S. Acharya, et al., Production of muons from heavy-flavour hadron decays at high transverse momentum in Pb-Pb collisions at $\sqrt{s_{\rm NN}} = 5.02$ and 2.76 TeV, Phys. Lett. B 820 (2021) 136558, arXiv:2011.05718 [nucl-ex].

[93] ALICE Collaboration, S. Acharya, et al., Production of muons from heavy-flavour hadron decays in pp collisions at $\sqrt{s}$ = 5.02 TeV, J. High Energy Phys. 09 (2019) 008, arXiv:1905.07207 [nucl-ex].

[94] ALICE Collaboration, B.B. Abelev, et al., Multiplicity dependence of jet-like two-particle correlation structures in p–Pb collisions at $\sqrt{s_{NN}}$=5.02 TeV, Phys. Lett. B 741 (2015) 38–50, arXiv:1406.5463 [nucl-ex].

[95] S. Roesler, R. Engel, J. Ranft, The Monte Carlo event generator DPMJET-III, in: International Conference on Advanced Monte Carlo for Radiation Physics, Particle Transport Simulation and Applications (MC 2000), 2000, pp. 1033–1038. 12, arXiv:hep-ph/0012252.

[96] GEANT4 Collaboration, S. Agostinelli, et al., GEANT4–a simulation toolkit, Nucl. Instrum. Methods, Sect. A 506 (2003) 250–303.

[97] GEANT4 Collaboration, M. Asai, A. Dotti, M. Verderi, D.H. Wright, Recent developments in Geant4, Ann. Nucl. Energy 82 (2015) 19–28.

[98] M. Masera, G. Ortona, M.G. Poghosyan, F. Prino, Anisotropic transverse flow introduction in Monte Carlo generators for heavy ion collisions, Phys. Rev. C 79 (2009) 064909.

[99] J. Xu, C.M. Ko, Pb-Pb collisions at $\sqrt{s_{\rm NN}} = 2.76$ TeV in a multiphase transport model, Phys. Rev. C 83 (2011) 034904, arXiv:1101.2231 [nucl-th].

[100] B. Efron, The Jackknife, the Bootstrap and Other Resampling Plans, CBMS-NSF Regional Conference Series in Applied Mathematics, SIAM, Philadelphia, PA, 1982, https://cds.cern.ch/record/98913, Lectures given at Bowling Green State Univ., June 1980.

[101] CMS Collaboration, V. Khachatryan, et al., Evidence for transverse momentum and pseudorapidity dependent event plane fluctuations in PbPb and pPb collisions, Phys. Rev. C 92 (2015) 034911, arXiv:1503.01692 [nucl-ex].

[102] ATLAS Collaboration, M. Aaboud, et al., Measurement of longitudinal flow decorrelations in Pb+Pb collisions at $\sqrt{s_{\rm NN}} = 2.76$ and 5.02 TeV with the ATLAS detector, Eur. Phys. J. C 78 (2018) 142, arXiv:1709.02301 [nucl-ex].

[103] ALICE Collaboration, S. Acharya, et al., Searches for transverse momentum dependent flow vector fluctuations in Pb–Pb and p–Pb collisions at the LHC, J. High Energy Phys. 09 (2017) 032, arXiv:1707.05690 [nucl-ex].

[104] ALICE Collaboration, S. Acharya, et al., Study of J/ψ azimuthal anisotropy at forward rapidity in Pb–Pb collisions at $\sqrt{s_{\rm NN}} = 5.02$ TeV, J. High Energy Phys. 02 (2019) 012, arXiv:1811.12727 [nucl-ex].

[105] M. Cacciari, M. Greco, P. Nason, The $p_{\rm T}$ spectrum in heavy flavor hadroproduction, J. High Energy Phys. 05 (1998) 007, arXiv:hep-ph/9803400 [hep-ph].

[106] M. Cacciari, S. Frixione, N. Houdeau, M.L. Mangano, P. Nason, G. Ridolfi, Theoretical predictions for charm and bottom production at the LHC, J. High Energy Phys. 10 (2012) 137, arXiv:1205.6344 [hep-ph].

[107] ALICE Collaboration, Centrality determination in heavy ion collisions, ALICE-PUBLIC-2018-011, http://cds.cern.ch/record/2636623, Aug. 2018.

[108] ALICE Collaboration, B.B. Abelev, et al., Long-range angular correlations of π, K and p in p-Pb collisions at $\sqrt{s_{\rm NN}}$ = 5.02 TeV, Phys. Lett. B 726 (2013) 164–177, arXiv:1307.3237 [nucl-ex].

[109] ALICE Collaboration, The ALICE experiment – a journey through QCD, arXiv:2211.04384 [nucl-ex].

[110] T. Sjöstrand, S. Ask, J.R. Christiansen, R. Corke, N. Desai, P. Ilten, S. Mrenna, S. Prestel, C.O. Rasmussen, P.Z. Skands, An introduction to PYTHIA 8.2, Comput. Phys. Commun. 191 (2015) 159–177, arXiv:1410.3012 [hep-ph].

[111] ALICE Collaboration, S. Acharya, et al., D-meson azimuthal anisotropy in midcentral Pb-Pb collisions at $\sqrt{s_{\rm NN}} = 5.02$ TeV, Phys. Rev. Lett. 120 (2018) 102301, arXiv:1707.01005 [nucl-ex].

[112] W. Zhao, C.M. Ko, Y.-X. Liu, G.-Y. Qin, H. Song, Probing the partonic degrees of freedom in high-multiplicity p–Pb collisions at $\sqrt{s_{\rm NN}}$ = 5.02 TeV, Phys. Rev. Lett. 125 (2020) 072301, arXiv:1911.00826 [nucl-th].

[113] C. Zhang, C. Marquet, G.-Y. Qin, S.-Y. Wei, B.-W. Xiao, Elliptic flow of heavy quarkonia in pA collisions, Phys. Rev. Lett. 122 (2019) 172302, arXiv:1901.10320 [hep-ph].

[114] C. Zhang, C. Marquet, G.-Y. Qin, Y. Shi, L. Wang, S.-Y. Wei, B.-W. Xiao, Collectivity of heavy mesons in proton-nucleus collisions, Phys. Rev. D 102 (2020) 034010, arXiv:2002.09878 [hep-ph].

[115] J.L. Albacete, C. Marquet, Single inclusive hadron production at RHIC and the LHC from the color glass condensate, Phys. Lett. B 687 (2010) 174–179, arXiv:1001.1378 [hep-ph].

ALICE Collaboration

S. Acharya [124], D. Adamová [85], A. Adler [69], G. Aglieri Rinella [32], M. Agnello [29], N. Agrawal [50], Z. Ahammed [132], S. Ahmad [15], S.U. Ahn [70], I. Ahuja [37], A. Akindinov [140], M. Al-Turany [96], D. Aleksandrov [140], B. Alessandro [55], H.M. Alfanda [6], R. Alfaro Molina [66], B. Ali [15], A. Alici [25], N. Alizadehvandchali [113], A. Alkin [32], J. Alme [20], G. Alocco [51], T. Alt [63], I. Altsybeev [140], M.N. Anaam [6], C. Andrei [45], A. Andronic [135], V. Anguelov [93], F. Antinori [53], P. Antonioli [50], N. Apadula [73], L. Aphecetche [102], H. Appelshäuser [63], C. Arata [72], S. Arcelli [25], M. Aresti [51], R. Arnaldi [55], I.C. Arsene [19], M. Arslandok [137], A. Augustinus [32], R. Averbeck [96], M.D. Azmi [15], A. Badalà [52], J. Bae [103], Y.W. Baek [40], X. Bai [117], R. Bailhache [63], Y. Bailung [47], A. Balbino [29], A. Baldisseri [127], B. Balis [2], D. Banerjee [4], Z. Banoo [90], R. Barbera [26], F. Barile [31], L. Barioglio [94], M. Barlou [77], G.G. Barnaföldi [136], L.S. Barnby [84], V. Barret [124], L. Barreto [109], C. Bartels [116], K. Barth [32], E. Bartsch [63], F. Baruffaldi [27], N. Bastid [124], S. Basu [74], G. Batigne [102], D. Battistini [94], B. Batyunya [141], D. Bauri [46], J.L. Bazo Alba [100], I.G. Bearden [82], C. Beattie [137], P. Becht [96], D. Behera [47], I. Belikov [126], A.D.C. Bell Hechavarria [135], F. Bellini [25], R. Bellwied [113], S. Belokurova [140], V. Belyaev [140], G. Bencedi [136], S. Beole [24], A. Bercuci [45], Y. Berdnikov [140], A. Berdnikova [93], L. Bergmann [93], M.G. Besoiu [62], L. Betev [32], P.P. Bhaduri [132], A. Bhasin [90], M.A. Bhat [4], B. Bhattacharjee [41], L. Bianchi [24], N. Bianchi [48], J. Bielčík [35], J. Bielčíková [85], J. Biernat [106], A.P. Bigot [126], A. Bilandzic [94], G. Biro [136], S. Biswas [4], N. Bize [102], J.T. Blair [107], D. Blau [140], M.B. Blidaru [96], N. Bluhme [38], C. Blume [63], G. Boca [21,54], F. Bock [86], T. Bodova [20], A. Bogdanov [140], S. Boi [22], J. Bok [57], L. Boldizsár [136], A. Bolozdynya [140], M. Bombara [37], P.M. Bond [32], G. Bonomi [131,54], H. Borel [127], A. Borissov [140], A.G. Borquez Carcamo [93], H. Bossi [137], E. Botta [24], Y.E.M. Bouziani [63], L. Bratrud [63], P. Braun-Munzinger [96], M. Bregant [109], M. Broz [35], G.E. Bruno [95,31], D. Budnikov [140], H. Buesching [63], S. Bufalino [29], O. Bugnon [102], P. Buhler [101], Z. Buthelezi [67,120], S.A. Bysiak [106], M. Cai [6], H. Caines [137], A. Caliva [96], E. Calvo Villar [100], J.M.M. Camacho [108], P. Camerini [23], F.D.M. Canedo [109], M. Carabas [123], A.A. Carballo [32], F. Carnesecchi [32], R. Caron [125], J. Castillo Castellanos [127], F. Catalano [24,29], C. Ceballos Sanchez [141], I. Chakaberia [73], P. Chakraborty [46], S. Chandra [132], S. Chapeland [32], M. Chartier [116], S. Chattopadhyay [132], S. Chattopadhyay [98], T.G. Chavez [44], T. Cheng [96,6], C. Cheshkov [125], B. Cheynis [125], V. Chibante Barroso [32], D.D. Chinellato [110], E.S. Chizzali [94,II], J. Cho [57], S. Cho [57], P. Chochula [32], P. Christakoglou [83], C.H. Christensen [82], P. Christiansen [74], T. Chujo [122], M. Ciacco [29], C. Cicalo [51], F. Cindolo [50], M.R. Ciupek [96], G. Clai [50,III], F. Colamaria [49], J.S. Colburn [99], D. Colella [95,31], M. Colocci [32], M. Concas [55,IV], G. Conesa Balbastre [72], Z. Conesa del Valle [128], G. Contin [23], J.G. Contreras [35], M.L. Coquet [127], T.M. Cormier [86,I], P. Cortese [130,55], M.R. Cosentino [111], F. Costa [32], S. Costanza [21,54], J. Crkovská [93], P. Crochet [124], R. Cruz-Torres [73], E. Cuautle [64], P. Cui [6], A. Dainese [53], M.C. Danisch [93], A. Danu [62], P. Das [79], P. Das [4], S. Das [4], A.R. Dash [135], S. Dash [46], R.M.H. David [44], A. De Caro [28], G. de Cataldo [49], J. de Cuveland [38], A. De Falco [22], D. De Gruttola [28], N. De Marco [55], C. De Martin [23], S. De Pasquale [28], S. Deb [47], R.J. Debski [2], K.R. Deja [133], R. Del Grande [94], L. Dello Stritto [28], W. Deng [6], P. Dhankher [18], D. Di Bari [31], A. Di Mauro [32], R.A. Diaz [141,7], T. Dietel [112], Y. Ding [125,6], R. Divià [32], D.U. Dixit [18], Ø. Djuvsland [20], U. Dmitrieva [140], A. Dobrin [62], B. Dönigus [63], J.M. Dubinski [133], A. Dubla [96],

S. Dudi [89], P. Dupieux [124], M. Durkac [105], N. Dzalaiova [12], T.M. Eder [135], R.J. Ehlers [86], V.N. Eikeland [20], F. Eisenhut [63], D. Elia [49], B. Erazmus [102], F. Ercolessi [25], F. Erhardt [88], M.R. Ersdal [20], B. Espagnon [128], G. Eulisse [32], D. Evans [99], S. Evdokimov [140], L. Fabbietti [94], M. Faggin [27], J. Faivre [72], F. Fan [6], W. Fan [73], A. Fantoni [48], M. Fasel [86], P. Fecchio [29], A. Feliciello [55], G. Feofilov [140], A. Fernández Téllez [44], L. Ferrandi [109], M.B. Ferrer [32], A. Ferrero [127], C. Ferrero [55], A. Ferretti [24], V.J.G. Feuillard [93], V. Filova [35], D. Finogeev [140], F.M. Fionda [51], F. Flor [113], A.N. Flores [107], S. Foertsch [67], I. Fokin [93], S. Fokin [140], E. Fragiacomo [56], E. Frajna [136], U. Fuchs [32], N. Funicello [28], C. Furget [72], A. Furs [140], T. Fusayasu [97], J.J. Gaardhøje [82], M. Gagliardi [24], A.M. Gago [100], C.D. Galvan [108], D.R. Gangadharan [113], P. Ganoti [77], C. Garabatos [96], J.R.A. Garcia [44], E. Garcia-Solis [9], K. Garg [102], C. Gargiulo [32], A. Garibli [80], K. Garner [135], P. Gasik [96], A. Gautam [115], M.B. Gay Ducati [65], M. Germain [102], C. Ghosh [132], M. Giacalone [25], P. Giubellino [96,55], P. Giubilato [27], A.M.C. Glaenzer [127], P. Glässel [93], E. Glimos [119], D.J.Q. Goh [75], V. Gonzalez [134], L.H. González-Trueba [66], M. Gorgon [2], S. Gotovac [33], V. Grabski [66], L.K. Graczykowski [133], E. Grecka [85], A. Grelli [58], C. Grigoras [32], V. Grigoriev [140], S. Grigoryan [141,1], F. Grosa [32], J.F. Grosse-Oetringhaus [32], R. Grosso [96], D. Grund [35], G.G. Guardiano [110], R. Guernane [72], M. Guilbaud [102], K. Gulbrandsen [82], T. Gündem [63], T. Gunji [121], W. Guo [6], A. Gupta [90], R. Gupta [90], S.P. Guzman [44], L. Gyulai [136], M.K. Habib [96], C. Hadjidakis [128], F.U. Haider [90], H. Hamagaki [75], A. Hamdi [73], M. Hamid [6], Y. Han [138], R. Hannigan [107], M.R. Haque [133], J.W. Harris [137], A. Harton [9], H. Hassan [86], D. Hatzifotiadou [50], P. Hauer [42], L.B. Havener [137], S.T. Heckel [94], E. Hellbär [96], H. Helstrup [34], M. Hemmer [63], T. Herman [35], G. Herrera Corral [8], F. Herrmann [135], S. Herrmann [125], K.F. Hetland [34], B. Heybeck [63], H. Hillemanns [32], C. Hills [116], B. Hippolyte [126], B. Hofman [58], B. Hohlweger [83], G.H. Hong [138], M. Horst [94], A. Horzyk [2], R. Hosokawa [14], Y. Hou [6], P. Hristov [32], C. Hughes [119], P. Huhn [63], L.M. Huhta [114], C.V. Hulse [128], T.J. Humanic [87], A. Hutson [113], D. Hutter [38], J.P. Iddon [116], R. Ilkaev [140], H. Ilyas [13], M. Inaba [122], G.M. Innocenti [32], M. Ippolitov [140], A. Isakov [85], T. Isidori [115], M.S. Islam [98], M. Ivanov [96], M. Ivanov [12], V. Ivanov [140], M. Jablonski [2], B. Jacak [73], N. Jacazio [32], P.M. Jacobs [73], S. Jadlovska [105], J. Jadlovsky [105], S. Jaelani [81], L. Jaffe [38], C. Jahnke [110], M.J. Jakubowska [133], M.A. Janik [133], T. Janson [69], M. Jercic [88], S. Jia [10], A.A.P. Jimenez [64], F. Jonas [86], J.M. Jowett [32,96], J. Jung [63], M. Jung [63], A. Junique [32], A. Jusko [99], M.J. Kabus [32,133], J. Kaewjai [104], P. Kalinak [59], A.S. Kalteyer [96], A. Kalweit [32], V. Kaplin [140], A. Karasu Uysal [71], D. Karatovic [88], O. Karavichev [140], T. Karavicheva [140], P. Karczmarczyk [133], E. Karpechev [140], U. Kebschull [69], R. Keidel [139], D.L.D. Keijdener [58], M. Keil [32], B. Ketzer [42], A.M. Khan [6], S. Khan [15], A. Khanzadeev [140], Y. Kharlov [140], A. Khatun [115,15], A. Khuntia [106], M.B. Kidson [112], B. Kileng [34], B. Kim [16], C. Kim [16], D.J. Kim [114], E.J. Kim [68], J. Kim [138], J.S. Kim [40], J. Kim [93], J. Kim [68], M. Kim [18,93], S. Kim [17], T. Kim [138], K. Kimura [91], S. Kirsch [63], I. Kisel [38], S. Kiselev [140], A. Kisiel [133], J.P. Kitowski [2], J.L. Klay [5], J. Klein [32], S. Klein [73], C. Klein-Bösing [135], M. Kleiner [63], T. Klemenz [94], A. Kluge [32], A.G. Knospe [113], C. Kobdaj [104], T. Kollegger [96], A. Kondratyev [141], E. Kondratyuk [140], J. Konig [63], S.A. Konigstorfer [94], P.J. Konopka [32], G. Kornakov [133], S.D. Koryciak [2], A. Kotliarov [85], V. Kovalenko [140], M. Kowalski [106], V. Kozhuharov [36], I. Králik [59], A. Kravčáková [37], L. Kreis [96], M. Krivda [99,59], F. Krizek [85], K. Krizkova Gajdosova [35],

M. Kroesen [93], M. Krüger [63], D.M. Krupova [35], E. Kryshen [140], V. Kučera [32], C. Kuhn [126], P.G. Kuijer [83], T. Kumaoka [122], D. Kumar [132], L. Kumar [89], N. Kumar [89], S. Kumar [31], S. Kundu [32], P. Kurashvili [78], A. Kurepin [140], A.B. Kurepin [140], A. Kuryakin [140], S. Kushpil [85], J. Kvapil [99], M.J. Kweon [57], J.Y. Kwon [57], Y. Kwon [138], S.L. La Pointe [38], P. La Rocca [26], Y.S. Lai [73], A. Lakrathok [104], M. Lamanna [32], R. Langoy [118], P. Larionov [32], E. Laudi [32], L. Lautner [32,94], R. Lavicka [101], T. Lazareva [140], R. Lea [131,54], H. Lee [103], G. Legras [135], J. Lehrbach [38], R.C. Lemmon [84], I. León Monzón [108], M.M. Lesch [94], E.D. Lesser [18], M. Lettrich [94], P. Lévai [136], X. Li [10], X.L. Li [6], J. Lien [118], R. Lietava [99], B. Lim [24,16], S.H. Lim [16], V. Lindenstruth [38], A. Lindner [45], C. Lippmann [96], A. Liu [18], D.H. Liu [6], J. Liu [116], I.M. Lofnes [20], C. Loizides [86], S. Lokos [106], P. Loncar [33], J.A. Lopez [93], X. Lopez [124], E. López Torres [7], P. Lu [96,117], J.R. Luhder [135], M. Lunardon [27], G. Luparello [56], Y.G. Ma [39], A. Maevskaya [140], M. Mager [32], T. Mahmoud [42], A. Maire [126], M.V. Makariev [36], M. Malaev [140], G. Malfattore [25], N.M. Malik [90], Q.W. Malik [19], S.K. Malik [90], L. Malinina [141,VII], D. Mal'Kevich [140], D. Mallick [79], N. Mallick [47], G. Mandaglio [30,52], V. Manko [140], F. Manso [124], V. Manzari [49], Y. Mao [6], G.V. Margagliotti [23], A. Margotti [50], A. Marín [96], C. Markert [107], P. Martinengo [32], J.L. Martinez [113], M.I. Martínez [44], G. Martínez García [102], S. Masciocchi [96], M. Masera [24], A. Masoni [51], L. Massacrier [128], A. Mastroserio [129,49], A.M. Mathis [94], O. Matonoha [74], P.F.T. Matuoka [109], A. Matyja [106], C. Mayer [106], A.L. Mazuecos [32], F. Mazzaschi [24], M. Mazzilli [32], J.E. Mdhluli [120], A.F. Mechler [63], Y. Melikyan [43,140], A. Menchaca-Rocha [66], E. Meninno [101,28], A.S. Menon [113], M. Meres [12], S. Mhlanga [112,67], Y. Miake [122], L. Micheletti [55], L.C. Migliorin [125], D.L. Mihaylov [94], K. Mikhaylov [141,140], A.N. Mishra [136], D. Miśkowiec [96], A. Modak [4], A.P. Mohanty [58], B. Mohanty [79], M. Mohisin Khan [15,V], M.A. Molander [43], Z. Moravcova [82], C. Mordasini [94], D.A. Moreira De Godoy [135], I. Morozov [140], A. Morsch [32], T. Mrnjavac [32], V. Muccifora [48], S. Muhuri [132], J.D. Mulligan [73], A. Mulliri [22], M.G. Munhoz [109], R.H. Munzer [63], H. Murakami [121], S. Murray [112], L. Musa [32], J. Musinsky [59], J.W. Myrcha [133], B. Naik [120], A.I. Nambrath [18], B.K. Nandi [46], R. Nania [50], E. Nappi [49], A.F. Nassirpour [74], A. Nath [93], C. Nattrass [119], M.N. Naydenov [36], A. Neagu [19], A. Negru [123], L. Nellen [64], S.V. Nesbo [34], G. Neskovic [38], D. Nesterov [140], B.S. Nielsen [82], E.G. Nielsen [82], S. Nikolaev [140], S. Nikulin [140], V. Nikulin [140], F. Noferini [50], S. Noh [11], P. Nomokonov [141], J. Norman [116], N. Novitzky [122], P. Nowakowski [133], A. Nyanin [140], J. Nystrand [20], M. Ogino [75], A. Ohlson [74], V.A. Okorokov [140], J. Oleniacz [133], A.C. Oliveira Da Silva [119], M.H. Oliver [137], A. Onnerstad [114], C. Oppedisano [55], A. Ortiz Velasquez [64], J. Otwinowski [106], M. Oya [91], K. Oyama [75], Y. Pachmayer [93], S. Padhan [46], D. Pagano [131,54], G. Paić [64], A. Palasciano [49], S. Panebianco [127], H. Park [122], H. Park [103], J. Park [57], J.E. Parkkila [32], R.N. Patra [90], B. Paul [22], H. Pei [6], T. Peitzmann [58], X. Peng [6], M. Pennisi [24], L.G. Pereira [65], D. Peresunko [140], G.M. Perez [7], S. Perrin [127], Y. Pestov [140], V. Petráček [35], V. Petrov [140], M. Petrovici [45], R.P. Pezzi [102,65], S. Piano [56], M. Pikna [12], P. Pillot [102], O. Pinazza [50,32], L. Pinsky [113], C. Pinto [94], S. Pisano [48], M. Płoskoń [73], M. Planinic [88], F. Pliquett [63], M.G. Poghosyan [86], B. Polichtchouk [140], S. Politano [29], N. Poljak [88], A. Pop [45], S. Porteboeuf-Houssais [124], V. Pozdniakov [141], K.K. Pradhan [47], S.K. Prasad [4], S. Prasad [47], R. Preghenella [50], F. Prino [55], C.A. Pruneau [134], I. Pshenichnov [140], M. Puccio [32], S. Pucillo [24], Z. Pugelova [105], S. Qiu [83], L. Quaglia [24], R.E. Quishpe [113], S. Ragoni [14,99], A. Rakotozafindrabe [127], L. Ramello [130,55],

F. Rami [126], S.A.R. Ramirez [44], T.A. Rancien [72], M. Rasa [26], S.S. Räsänen [43], R. Rath [50,47], M.P. Rauch [20], I. Ravasenga [83], K.F. Read [86,119], C. Reckziegel [111], A.R. Redelbach [38], K. Redlich [78,VI], A. Rehman [20], F. Reidt [32], H.A. Reme-Ness [34], Z. Rescakova [37], K. Reygers [93], A. Riabov [140], V. Riabov [140], R. Ricci [28], M. Richter [19], A.A. Riedel [94], W. Riegler [32], C. Ristea [62], M. Rodríguez Cahuantzi [44], K. Røed [19], R. Rogalev [140], E. Rogochaya [141], T.S. Rogoschinski [63], D. Rohr [32], D. Röhrich [20], P.F. Rojas [44], S. Rojas Torres [35], P.S. Rokita [133], G. Romanenko [141], F. Ronchetti [48], A. Rosano [30,52], E.D. Rosas [64], A. Rossi [53], A. Roy [47], S. Roy [46], N. Rubini [25], D. Ruggiano [133], R. Rui [23], B. Rumyantsev [141], P.G. Russek [2], R. Russo [83], A. Rustamov [80], E. Ryabinkin [140], Y. Ryabov [140], A. Rybicki [106], H. Rytkonen [114], W. Rzesa [133], O.A.M. Saarimaki [43], R. Sadek [102], S. Sadhu [31], S. Sadovsky [140], J. Saetre [20], K. Šafařík [35], S.K. Saha [4], S. Saha [79], B. Sahoo [46], R. Sahoo [47], S. Sahoo [60], D. Sahu [47], P.K. Sahu [60], J. Saini [132], K. Sajdakova [37], S. Sakai [122], M.P. Salvan [96], S. Sambyal [90], I. Sanna [32,94], T.B. Saramela [109], D. Sarkar [134], N. Sarkar [132], P. Sarma [41], V. Sarritzu [22], V.M. Sarti [94], M.H.P. Sas [137], J. Schambach [86], H.S. Scheid [63], C. Schiaua [45], R. Schicker [93], A. Schmah [93], C. Schmidt [96], H.R. Schmidt [92], M.O. Schmidt [32], M. Schmidt [92], N.V. Schmidt [86], A.R. Schmier [119], R. Schotter [126], A. Schröter [38], J. Schukraft [32], K. Schwarz [96], K. Schweda [96], G. Scioli [25], E. Scomparin [55], J.E. Seger [14], Y. Sekiguchi [121], D. Sekihata [121], I. Selyuzhenkov [96,140], S. Senyukov [126], J.J. Seo [57], D. Serebryakov [140], L. Šerkšnytė [94], A. Sevcenco [62], T.J. Shaba [67], A. Shabetai [102], R. Shahoyan [32], A. Shangaraev [140], A. Sharma [89], D. Sharma [46], H. Sharma [106], M. Sharma [90], S. Sharma [75], S. Sharma [90], U. Sharma [90], A. Shatat [128], O. Sheibani [113], K. Shigaki [91], M. Shimomura [76], J. Shin [11], S. Shirinkin [140], Q. Shou [39], Y. Sibiriak [140], S. Siddhanta [51], T. Siemiarczuk [78], T.F. Silva [109], D. Silvermyr [74], T. Simantathammakul [104], R. Simeonov [36], B. Singh [90], B. Singh [94], R. Singh [79], R. Singh [90], R. Singh [47], S. Singh [15], V.K. Singh [132], V. Singhal [132], T. Sinha [98], B. Sitar [12], M. Sitta [130,55], T.B. Skaali [19], G. Skorodumovs [93], M. Slupecki [43], N. Smirnov [137], R.J.M. Snellings [58], E.H. Solheim [19], J. Song [113], A. Songmoolnak [104], F. Soramel [27], R. Spijkers [83], I. Sputowska [106], J. Staa [74], J. Stachel [93], I. Stan [62], P.J. Steffanic [119], S.F. Stiefelmaier [93], D. Stocco [102], I. Storehaug [19], P. Stratmann [135], S. Strazzi [25], C.P. Stylianidis [83], A.A.P. Suaide [109], C. Suire [128], M. Sukhanov [140], M. Suljic [32], R. Sultanov [140], V. Sumberia [90], S. Sumowidagdo [81], S. Swain [60], I. Szarka [12], S.F. Taghavi [94], G. Taillepied [96], J. Takahashi [110], G.J. Tambave [20], S. Tang [124,6], Z. Tang [117], J.D. Tapia Takaki [115], N. Tapus [123], L.A. Tarasovicova [135], M.G. Tarzila [45], G.F. Tassielli [31], A. Tauro [32], G. Tejeda Muñoz [44], A. Telesca [32], L. Terlizzi [24], C. Terrevoli [113], G. Tersimonov [3], S. Thakur [4], D. Thomas [107], A. Tikhonov [140], A.R. Timmins [113], M. Tkacik [105], T. Tkacik [105], A. Toia [63], R. Tokumoto [91], N. Topilskaya [140], M. Toppi [48], F. Torales-Acosta [18], T. Tork [128], A.G. Torres Ramos [31], A. Trifiró [30,52], A.S. Triolo [30,52], S. Tripathy [50], T. Tripathy [46], S. Trogolo [32], V. Trubnikov [3], W.H. Trzaska [114], T.P. Trzcinski [133], A. Tumkin [140], R. Turrisi [53], T.S. Tveter [19], K. Ullaland [20], B. Ulukutlu [94], A. Uras [125], M. Urioni [54,131], G.L. Usai [22], M. Vala [37], N. Valle [21], L.V.R. van Doremalen [58], M. van Leeuwen [83], C.A. van Veen [93], R.J.G. van Weelden [83], P. Vande Vyvre [32], D. Varga [136], Z. Varga [136], M. Vasileiou [77], A. Vasiliev [140], O. Vázquez Doce [48], O. Vazquez Rueda [113,74], V. Vechernin [140], E. Vercellin [24], S. Vergara Limón [44], L. Vermunt [96], R. Vértesi [136], M. Verweij [58], L. Vickovic [33], Z. Vilakazi [120], O. Villalobos Baillie [99], G. Vino [49],

A. Vinogradov [140], T. Virgili [28], V. Vislavicius [82], A. Vodopyanov [141], B. Volkel [32], M.A. Völkl [93], K. Voloshin [140], S.A. Voloshin [134], G. Volpe [31], B. von Haller [32], I. Vorobyev [94], N. Vozniuk [140], J. Vrláková [37], C. Wang [39], D. Wang [39], Y. Wang [39], A. Wegrzynek [32], F.T. Weiglhofer [38], S.C. Wenzel [32], J.P. Wessels [135], S.L. Weyhmiller [137], J. Wiechula [63], J. Wikne [19], G. Wilk [78], J. Wilkinson [96], G.A. Willems [135], B. Windelband [93], M. Winn [127], J.R. Wright [107], W. Wu [39], Y. Wu [117], R. Xu [6], A. Yadav [42], A.K. Yadav [132], S. Yalcin [71], Y. Yamaguchi [91], K. Yamakawa [91], S. Yang [20], S. Yano [91], Z. Yin [6], I.-K. Yoo [16], J.H. Yoon [57], S. Yuan [20], A. Yuncu [93], V. Zaccolo [23], C. Zampolli [32], F. Zanone [93], N. Zardoshti [32,99], A. Zarochentsev [140], P. Závada [61], N. Zaviyalov [140], M. Zhalov [140], B. Zhang [6], L. Zhang [39], S. Zhang [39], X. Zhang [6], Y. Zhang [117], Z. Zhang [6], M. Zhao [10], V. Zherebchevskii [140], Y. Zhi [10], D. Zhou [6], Y. Zhou [82], J. Zhu [96,6], Y. Zhu [6], S.C. Zugravel [55], N. Zurlo [131,54]

[1] *A.I. Alikhanyan National Science Laboratory (Yerevan Physics Institute) Foundation, Yerevan, Armenia*
[2] *AGH University of Krakow, Cracow, Poland*
[3] *Bogolyubov Institute for Theoretical Physics, National Academy of Sciences of Ukraine, Kiev, Ukraine*
[4] *Bose Institute, Department of Physics and Centre for Astroparticle Physics and Space Science (CAPSS), Kolkata, India*
[5] *California Polytechnic State University, San Luis Obispo, CA, United States*
[6] *Central China Normal University, Wuhan, China*
[7] *Centro de Aplicaciones Tecnológicas y Desarrollo Nuclear (CEADEN), Havana, Cuba*
[8] *Centro de Investigación y de Estudios Avanzados (CINVESTAV), Mexico City and Mérida, Mexico*
[9] *Chicago State University, Chicago, IL, United States*
[10] *China Institute of Atomic Energy, Beijing, China*
[11] *Chungbuk National University, Cheongju, Republic of Korea*
[12] *Comenius University Bratislava, Faculty of Mathematics, Physics and Informatics, Bratislava, Slovak Republic*
[13] *COMSATS University Islamabad, Islamabad, Pakistan*
[14] *Creighton University, Omaha, NE, United States*
[15] *Department of Physics, Aligarh Muslim University, Aligarh, India*
[16] *Department of Physics, Pusan National University, Pusan, Republic of Korea*
[17] *Department of Physics, Sejong University, Seoul, Republic of Korea*
[18] *Department of Physics, University of California, Berkeley, CA, United States*
[19] *Department of Physics, University of Oslo, Oslo, Norway*
[20] *Department of Physics and Technology, University of Bergen, Bergen, Norway*
[21] *Dipartimento di Fisica, Università di Pavia, Pavia, Italy*
[22] *Dipartimento di Fisica dell'Università and Sezione INFN, Cagliari, Italy*
[23] *Dipartimento di Fisica dell'Università and Sezione INFN, Trieste, Italy*
[24] *Dipartimento di Fisica dell'Università and Sezione INFN, Turin, Italy*
[25] *Dipartimento di Fisica e Astronomia dell'Università and Sezione INFN, Bologna, Italy*
[26] *Dipartimento di Fisica e Astronomia dell'Università and Sezione INFN, Catania, Italy*
[27] *Dipartimento di Fisica e Astronomia dell'Università and Sezione INFN, Padova, Italy*
[28] *Dipartimento di Fisica 'E.R. Caianiello' dell'Università and Gruppo Collegato INFN, Salerno, Italy*
[29] *Dipartimento DISAT del Politecnico and Sezione INFN, Turin, Italy*
[30] *Dipartimento di Scienze MIFT, Università di Messina, Messina, Italy*
[31] *Dipartimento Interateneo di Fisica 'M. Merlin' and Sezione INFN, Bari, Italy*
[32] *European Organization for Nuclear Research (CERN), Geneva, Switzerland*
[33] *Faculty of Electrical Engineering, Mechanical Engineering and Naval Architecture, University of Split, Split, Croatia*
[34] *Faculty of Engineering and Science, Western Norway University of Applied Sciences, Bergen, Norway*
[35] *Faculty of Nuclear Sciences and Physical Engineering, Czech Technical University in Prague, Prague, Czech Republic*
[36] *Faculty of Physics, Sofia University, Sofia, Bulgaria*
[37] *Faculty of Science, P.J. Šafárik University, Košice, Slovak Republic*
[38] *Frankfurt Institute for Advanced Studies, Johann Wolfgang Goethe-Universität Frankfurt, Frankfurt, Germany*
[39] *Fudan University, Shanghai, China*
[40] *Gangneung-Wonju National University, Gangneung, Republic of Korea*
[41] *Gauhati University, Department of Physics, Guwahati, India*
[42] *Helmholtz-Institut für Strahlen- und Kernphysik, Rheinische Friedrich-Wilhelms-Universität Bonn, Bonn, Germany*
[43] *Helsinki Institute of Physics (HIP), Helsinki, Finland*
[44] *High Energy Physics Group, Universidad Autónoma de Puebla, Puebla, Mexico*
[45] *Horia Hulubei National Institute of Physics and Nuclear Engineering, Bucharest, Romania*
[46] *Indian Institute of Technology Bombay (IIT), Mumbai, India*
[47] *Indian Institute of Technology Indore, Indore, India*
[48] *INFN, Laboratori Nazionali di Frascati, Frascati, Italy*
[49] *INFN, Sezione di Bari, Bari, Italy*
[50] *INFN, Sezione di Bologna, Bologna, Italy*
[51] *INFN, Sezione di Cagliari, Cagliari, Italy*
[52] *INFN, Sezione di Catania, Catania, Italy*
[53] *INFN, Sezione di Padova, Padova, Italy*
[54] *INFN, Sezione di Pavia, Pavia, Italy*
[55] *INFN, Sezione di Torino, Turin, Italy*
[56] *INFN, Sezione di Trieste, Trieste, Italy*
[57] *Inha University, Incheon, Republic of Korea*
[58] *Institute for Gravitational and Subatomic Physics (GRASP), Utrecht University/Nikhef, Utrecht, Netherlands*

[59] Institute of Experimental Physics, Slovak Academy of Sciences, Košice, Slovak Republic
[60] Institute of Physics, Homi Bhabha National Institute, Bhubaneswar, India
[61] Institute of Physics of the Czech Academy of Sciences, Prague, Czech Republic
[62] Institute of Space Science (ISS), Bucharest, Romania
[63] Institut für Kernphysik, Johann Wolfgang Goethe-Universität Frankfurt, Frankfurt, Germany
[64] Instituto de Ciencias Nucleares, Universidad Nacional Autónoma de México, Mexico City, Mexico
[65] Instituto de Física, Universidade Federal do Rio Grande do Sul (UFRGS), Porto Alegre, Brazil
[66] Instituto de Física, Universidad Nacional Autónoma de México, Mexico City, Mexico
[67] iThemba LABS, National Research Foundation, Somerset West, South Africa
[68] Jeonbuk National University, Jeonju, Republic of Korea
[69] Johann-Wolfgang-Goethe Universität Frankfurt Institut für Informatik, Fachbereich Informatik und Mathematik, Frankfurt, Germany
[70] Korea Institute of Science and Technology Information, Daejeon, Republic of Korea
[71] KTO Karatay University, Konya, Turkey
[72] Laboratoire de Physique Subatomique et de Cosmologie, Université Grenoble-Alpes, CNRS-IN2P3, Grenoble, France
[73] Lawrence Berkeley National Laboratory, Berkeley, CA, United States
[74] Lund University Department of Physics, Division of Particle Physics, Lund, Sweden
[75] Nagasaki Institute of Applied Science, Nagasaki, Japan
[76] Nara Women's University (NWU), Nara, Japan
[77] National and Kapodistrian University of Athens, School of Science, Department of Physics, Athens, Greece
[78] National Centre for Nuclear Research, Warsaw, Poland
[79] National Institute of Science Education and Research, Homi Bhabha National Institute, Jatni, India
[80] National Nuclear Research Center, Baku, Azerbaijan
[81] National Research and Innovation Agency – BRIN, Jakarta, Indonesia
[82] Niels Bohr Institute, University of Copenhagen, Copenhagen, Denmark
[83] Nikhef, National institute for subatomic physics, Amsterdam, Netherlands
[84] Nuclear Physics Group, STFC Daresbury Laboratory, Daresbury, United Kingdom
[85] Nuclear Physics Institute of the Czech Academy of Sciences, Husinec-Řež, Czech Republic
[86] Oak Ridge National Laboratory, Oak Ridge, TN, United States
[87] Ohio State University, Columbus, OH, United States
[88] Physics department, Faculty of science, University of Zagreb, Zagreb, Croatia
[89] Physics Department, Panjab University, Chandigarh, India
[90] Physics Department, University of Jammu, Jammu, India
[91] Physics Program and International Institute for Sustainability with Knotted Chiral Meta Matter (SKCM2), Hiroshima University, Hiroshima, Japan
[92] Physikalisches Institut, Eberhard-Karls-Universität Tübingen, Tübingen, Germany
[93] Physikalisches Institut, Ruprecht-Karls-Universität Heidelberg, Heidelberg, Germany
[94] Physik Department, Technische Universität München, Munich, Germany
[95] Politecnico di Bari and Sezione INFN, Bari, Italy
[96] Research Division and ExtreMe Matter Institute EMMI, GSI Helmholtzzentrum für Schwerionenforschung GmbH, Darmstadt, Germany
[97] Saga University, Saga, Japan
[98] Saha Institute of Nuclear Physics, Homi Bhabha National Institute, Kolkata, India
[99] School of Physics and Astronomy, University of Birmingham, Birmingham, United Kingdom
[100] Sección Física, Departamento de Ciencias, Pontificia Universidad Católica del Perú, Lima, Peru
[101] Stefan Meyer Institut für Subatomare Physik (SMI), Vienna, Austria
[102] SUBATECH, IMT Atlantique, Nantes Université, CNRS-IN2P3, Nantes, France
[103] Sungkyunkwan University, Suwon City, Republic of Korea
[104] Suranaree University of Technology, Nakhon Ratchasima, Thailand
[105] Technical University of Košice, Košice, Slovak Republic
[106] The Henryk Niewodniczanski Institute of Nuclear Physics, Polish Academy of Sciences, Cracow, Poland
[107] The University of Texas at Austin, Austin, TX, United States
[108] Universidad Autónoma de Sinaloa, Culiacán, Mexico
[109] Universidade de São Paulo (USP), São Paulo, Brazil
[110] Universidade Estadual de Campinas (UNICAMP), Campinas, Brazil
[111] Universidade Federal do ABC, Santo Andre, Brazil
[112] University of Cape Town, Cape Town, South Africa
[113] University of Houston, Houston, TX, United States
[114] University of Jyväskylä, Jyväskylä, Finland
[115] University of Kansas, Lawrence, KS, United States
[116] University of Liverpool, Liverpool, United Kingdom
[117] University of Science and Technology of China, Hefei, China
[118] University of South-Eastern Norway, Kongsberg, Norway
[119] University of Tennessee, Knoxville, TN, United States
[120] University of the Witwatersrand, Johannesburg, South Africa
[121] University of Tokyo, Tokyo, Japan
[122] University of Tsukuba, Tsukuba, Japan
[123] University Politehnica of Bucharest, Bucharest, Romania
[124] Université Clermont Auvergne, CNRS/IN2P3, LPC, Clermont-Ferrand, France
[125] Université de Lyon, CNRS/IN2P3, Institut de Physique des 2 Infinis de Lyon, Lyon, France
[126] Université de Strasbourg, CNRS, IPHC UMR 7178, F-67000 Strasbourg, France
[127] Université Paris-Saclay, Centre d'Etudes de Saclay (CEA), IRFU, Département de Physique Nucléaire (DPhN), Saclay, France
[128] Université Paris-Saclay, CNRS/IN2P3, IJCLab, Orsay, France
[129] Università degli Studi di Foggia, Foggia, Italy
[130] Università del Piemonte Orientale, Vercelli, Italy
[131] Università di Brescia, Brescia, Italy
[132] Variable Energy Cyclotron Centre, Homi Bhabha National Institute, Kolkata, India
[133] Warsaw University of Technology, Warsaw, Poland
[134] Wayne State University, Detroit, MI, United States
[135] Westfälische Wilhelms-Universität Münster, Institut für Kernphysik, Münster, Germany
[136] Wigner Research Centre for Physics, Budapest, Hungary
[137] Yale University, New Haven, CT, United States
[138] Yonsei University, Seoul, Republic of Korea

[139] *Zentrum für Technologie und Transfer (ZTT), Worms, Germany*
[140] *Affiliated with an institute covered by a cooperation agreement with CERN*
[141] *Affiliated with an international laboratory covered by a cooperation agreement with CERN*

[I] Deceased.
[II] Also at: Max-Planck-Institut für Physik, Munich, Germany.
[III] Also at: Italian National Agency for New Technologies, Energy and Sustainable Economic Development (ENEA), Bologna, Italy.
[IV] Also at: Dipartimento DET del Politecnico di Torino, Turin, Italy.
[V] Also at: Department of Applied Physics, Aligarh Muslim University, Aligarh, India.
[VI] Also at: Institute of Theoretical Physics, University of Wroclaw, Poland.
[VII] Also at: An institution covered by a cooperation agreement with CERN.